AGU PUBLICATIONS

JGR

Journal of Geophysical Research: Space Physics

RESEARCH ARTICLE
10.1002/2014JA020228

Key Points:
- Plasmaspheric drainage plumes can persist for weeks
- The source of the plasma supplying the long-lived plumes is unknown
- Candidate sources include outflow from the tongue of ionization

Correspondence to:
J. E. Borovsky,
jborovsky@spacescience.org

Citation:
Borovsky, J. E., D. T. Welling, M. F. Thomsen, and M. H. Denton (2014), Long-lived plasmaspheric drainage plumes: Where does the plasma come from?, *J. Geophys. Res. Space Physics*, *119*, 6496–6520, doi:10.1002/2014JA020228.

Received 28 MAY 2014
Accepted 4 AUG 2014
Accepted article online 11 AUG 2014
Published online 26 AUG 2014

Long-lived plasmaspheric drainage plumes: Where does the plasma come from?

Joseph E. Borovsky[1,2,3], Daniel T. Welling[2], Michelle F. Thomsen[4], and Michael H. Denton[1,3]

[1]Center for Space Plasma Physics, Space Science Institute, Boulder, Colorado, USA, [2]AOSS, University of Michigan, Ann Arbor, Michigan, USA, [3]Department of Physics, Lancaster University, Lancaster, Lancashire, UK, [4]Planetary Science Institute, Tucson, Arizona, USA

Abstract Long-lived (weeks) plasmaspheric drainage plumes are explored. The long-lived plumes occur during long-lived high-speed-stream-driven storms. Spacecraft in geosynchronous orbit see the plumes as dense plasmaspheric plasma advecting sunward toward the dayside magnetopause. The older plumes have the same densities and local time widths as younger plumes, and like younger plumes they are lumpy in density and they reside in a spatial gap in the electron plasma sheet (in sort of a drainage corridor). Magnetospheric-convection simulations indicate that drainage from a filled outer plasmasphere can only supply a plume for 1.5–2 days. The question arises for long-lived plumes (and for any plume older than about 2 days): Where is the plasma coming from? Three candidate sources appear promising: (1) substorm disruption of the nightside plasmasphere which may transport plasmaspheric plasma outward onto open drift orbits, (2) radial transport of plasmaspheric plasma in velocity-shear-driven instabilities near the duskside plasmapause, and (3) an anomalously high upflux of cold ionospheric protons from the tongue of ionization in the dayside ionosphere, which may directly supply ionospheric plasma into the plume. In the first two cases the plume is drainage of plasma from the magnetosphere; in the third case it is not. Where the plasma in long-lived plumes is coming from is a quandary: to fix this dilemma, further work and probably full-scale simulations are needed.

1. Introduction

When the *Kp* index becomes elevated, a plume of plasmaspheric plasma is seen at all L shells in the dayside magnetosphere [*Chappell et al*., 1971; *Spiro et al*., 1981; *Carpenter et al*., 1993; *Elphic et al*., 1997; *Goldstein and Sandel*, 2005; *Sandel and Denton*, 2007]. This cold plasma is convecting sunward [*Borovsky et al*., 1998; *Matsui et al*., 1999; *Borovsky and Denton*, 2008] and will flow into the dayside reconnection site [*Borovsky et al*., 1997; *Su et al*., 2000; *McFadden et al*., 2008] where it can play an important role in mass loading the dayside reconnection rate during geomagnetically active times [*Borovsky and Steinberg*, 2006; *Borovsky and Denton*, 2006a; *Walsh et al*., 2013, 2014; *Borovsky et al*., 2013; *Borovsky*, 2014]. The plasmaspheric plume is also the site of enhanced pitch angle scattering of radiation belt electrons during geomagnetically active times [*Spasojevic et al*., 2004; *Fraser et al*., 2006; *Bortnik et al*., 2006; *Yahnin and Yahnina*, 2007; *Millan and Thorne*, 2007; *Jordanova et al*., 2007; *Borovsky et al*., 2014]. On the first day of a storm (when *Kp* is initially elevated) the plasmaspheric plume is very wide in local time as the outer plasmasphere surges toward the dayside magnetopause [*Chen and Wolf*, 1972; *Goldstein*, 2006; *Denton and Borovsky*, 2008; *Borovsky et al*., 2013], and the plasmaspheric plume narrows after the first day. The expectation is that this plume is composed of plasma being drained from the reservoir of plasmaspheric plasma that had been residing in the near-Earth magnetosphere [*Grebowsky*, 1970; *Chen and Wolf*, 1972; *Elphic et al*., 1996; *Weiss et al*., 1997]; i.e., it is thought that the plasmaspheric plume is drainage from the outer plasmasphere.

As will be seen in this report (and seen also in *Borovsky et al*. [2013]), the plasmaspheric drainage plume exists in a spatial (local time) gap in the electron plasma sheet in the dayside magnetosphere. And as is well known, the plasma of the plume is highly structured (lumpy) [*Spasojevic et al*., 2003; *Goldstein et al*., 2004; *Borovsky and Denton*, 2008; *Matsui et al*., 2012], to the point of being irregular. For these two reasons, an improved name for the "plasmaspheric drainage plume" might be "plasmaspheric drainage corridor" (C. R. Chappell, private communication, 2014). Both terminologies will be used here.

A survey of plasmaspheric plumes during the first 3.5 days of high-speed-stream-driven storms found that it is common for plasmaspheric plumes to last 3.5 days [cf. *Borovsky and Denton*, 2008, Figure 7]; this was the maximum length of time over which they were surveyed. An example of a plasmaspheric plume lasting

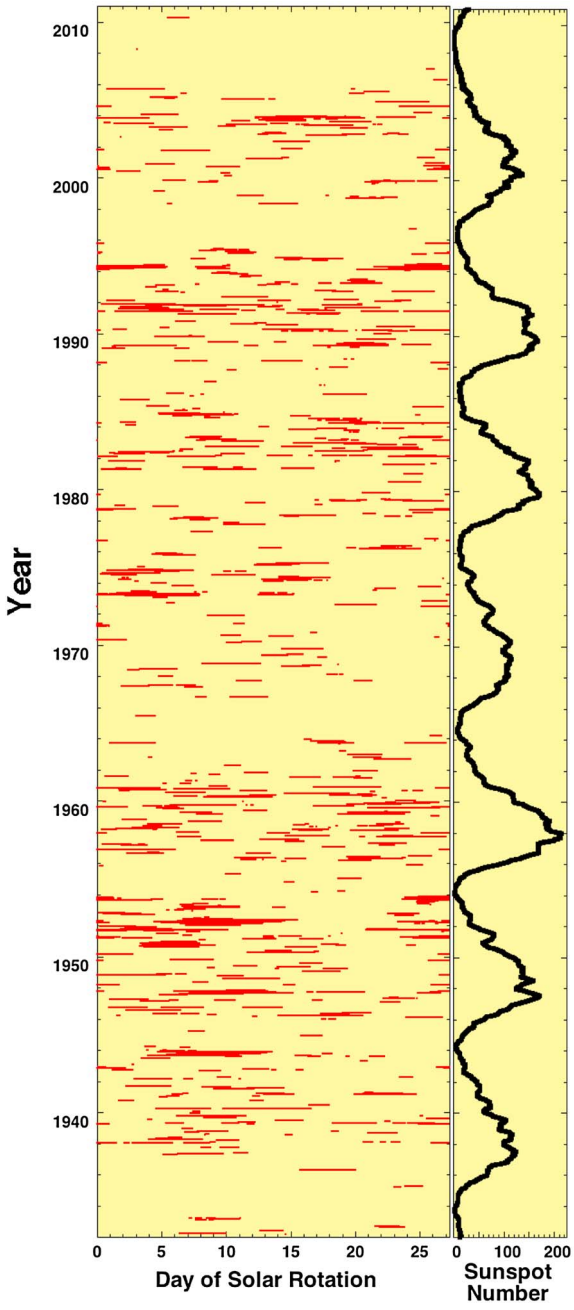

Figure 1. (left) In red are times when the 72 h average of *Kp* is greater than or equal to 4.0. (right) A 6 month running average of the sunspot number is plotted. Large concentrations occurred declining phases of the solar cycles of the 1950s, the 1970s, and the 1990s, perhaps following the 22 year magnetic solar cycle.

7 days can be seen in Figure 13 of *Borovsky et al.* [2013]. Plumes lasting this long (and longer) raise questions about how long it takes to completely drain the outer plasmasphere and whether these long-lived plumes have the same properties as younger plumes. In the present paper an analysis of these long-lived plumes will raise the question about where the plasma in the long-lived plumes comes from: whether it is drainage of plasmaspheric plasma that has been residing in the magnetosphere or whether it is fresh ionospheric outflow. It turns out that the question applies to all plumes lasting more than about 2 days.

As will be demonstrated in this report, whenever *Kp* is elevated, a plasmaspheric plume of sunward flowing cold plasma can be found crossing geosynchronous orbit in the dayside magnetosphere. Typical high-speed-stream-driven storms have durations of a few to several days, depending on the duration of the high-speed coronal-hole-origin solar wind that follows the corotating interaction region. There are, however, long-duration storms with *Kp* elevated for a week or two; during these long-durations storms long-lived plumes can be found.

During the declining phase of the solar cycle, equatorward extensions of coronal holes on the Sun can have geometries that result in long-lived high-speed wind at Earth [e.g., *McAllister et al.*, 1996]. If the toward away nature of the magnetic field in this coronal hole is Russell-McPherron effective [*McPherron et al.*, 2009], *Kp* can remain elevated for a week or more. In Figure 1 (left) times of long-term elevated *Kp* are plotted as a function of solar rotation for the years 1932–2011 (see also Figure 15 of *Borovsky and Denton* [2006b]); intervals where the 72 h running average of *Kp* is above 4.0 are indicated in red. In Figure 1 (right) the sunspot number is plotted. As can be seen, the long-duration red regions can be present during all phases of the solar cycle but are infrequent during solar minimum and are particularly prominent during the declining phase of the solar cycle. Note in Figure 1 (left) that every other declining phase appears well organized (e.g., 1950s, 1970s, 1990s), forming a 22 year pattern where the long intervals of *Kp* are more prevalent. During these intervals, very long lived plasmaspheric plumes can be found.

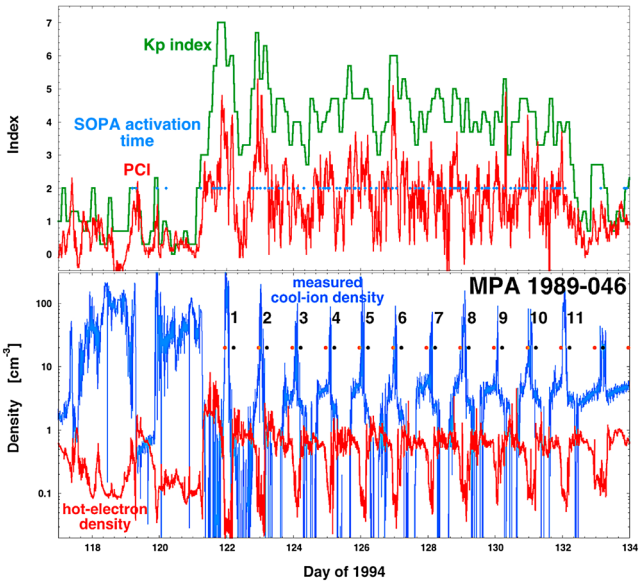

Figure 2. For a long-duration geomagnetic storm in May 1994 that has a calm before the storm, a drainage plume lasting 11 days is shown. (top) The *Kp* index (green) and PCI (red) are plotted and the times of substorm injections are denoted with blue dots. (bottom) The cold-ion density and hot-electron density measured by the spacecraft 1989–046 in geosynchronous orbit are plotted (logarithmically). The times at which 1989–046 crosses local noon are indicated by the orange dots, and the times at which it crosses 18 LT are indicated by the black dots. The plume crossing number is indicated by the black number.

Very long lived plumes are rare, but they highlight issues that are not understood about the plasmasphere and the plumes. In this report long-lived plasmaspheric plumes as seen by multiple spacecraft in geosynchronous orbit will be studied and numerical simulations will be used to investigate the drainage of the outer plasmasphere.

This report is organized as follows. In section 2 a long-lived (11 day) plasmaspheric plume from a long-duration storm with a calm before the storm is examined. In section 3 a long-lived (15 days) plasmaspheric plume from a long-duration storm without a calm before the storm is examined. In section 4 computer simulations are performed to determine how long it takes to drain the outer plasmasphere during a storm. In section 5 three potential sources for the plasma in the long-lived plumes are explored. Section 5.1 investigates the question of whether the plasma in long-lived plumes could be coming from radial diffusion out of the inner plasmasphere. Section 5.2 investigates the question of whether the plasma in long-lived plumes could be the result of substorms disrupting the nightside plasmapause. Section 5.3 investigates the question of whether the plasma in long-lived plumes could be coming from radial transport out of the inner plasmasphere by interchange instabilities. Section 5.4 investigates the question of whether the plasma in long-lived plumes could be coming from radial transport by velocity-shear-driven instabilities. In section 5.5 estimates are performed to determine whether enhanced plasmaspheric refilling rates above the tongue of ionization in the high-latitude dayside ionosphere could be directly feeding plasma to the plumes The results are summarized in section 6, a brief discussion about previous results is made in section 7, and a call for new research is made in section 8. In the Appendix A the question is addressed: Could convection be strengthening with time during the storms?

2. Observations of Long-Lived Plasmaspheric Plumes

An example from May 1994 of a plasmaspheric plume lasting 11 days is shown in Figure 2. The event is associated with high-speed solar wind emanating from an equatorward extension of a large southern polar coronal hole [cf. *McAllister et al.*, 1996]. In Figure 2 (top) the *Kp* index is plotted for 17 days as the green curve and the polar cap index (PCI) is plotted as the red curve. The times of substorm injections of energetic electrons into geosynchronous orbit, as determined from the multisatellite Synchronous Orbit Particle Analyzer (SOPA) data set [*Belian et al.*, 1992; *Cayton and Belian*, 2007], are plotted as the blue dots, with one blue dot per injection event. During Days 117–120 geomagnetic activity is low (the calm before the storm). During the first half of Day 121 geomagnetic activity rises from calm levels to storm levels. From Day 121.5 to Day 132.2 geomagnetic activity remains elevated at $Kp = 3$ or above. On Day 132.2 activity decreases to quiet levels.

In Figure 2 (bottom) the cold-ion density at geosynchronous orbit as measured by the Magnetospheric Plasma Analyzer (MPA) instrument [*Bame et al.*, 1993; *Thomsen et al.*, 1999] on the spacecraft 1989–046 in geosynchronous orbit is plotted in blue for the same 17 days in 1994. Note that the vertical axis in Figure 2 (bottom) is logarithmic. During Days 118–120 the outer plasmasphere is filled out to geosynchronous orbit and beyond, as indicated by dense cold plasma seen at all local times as the spacecraft travels in

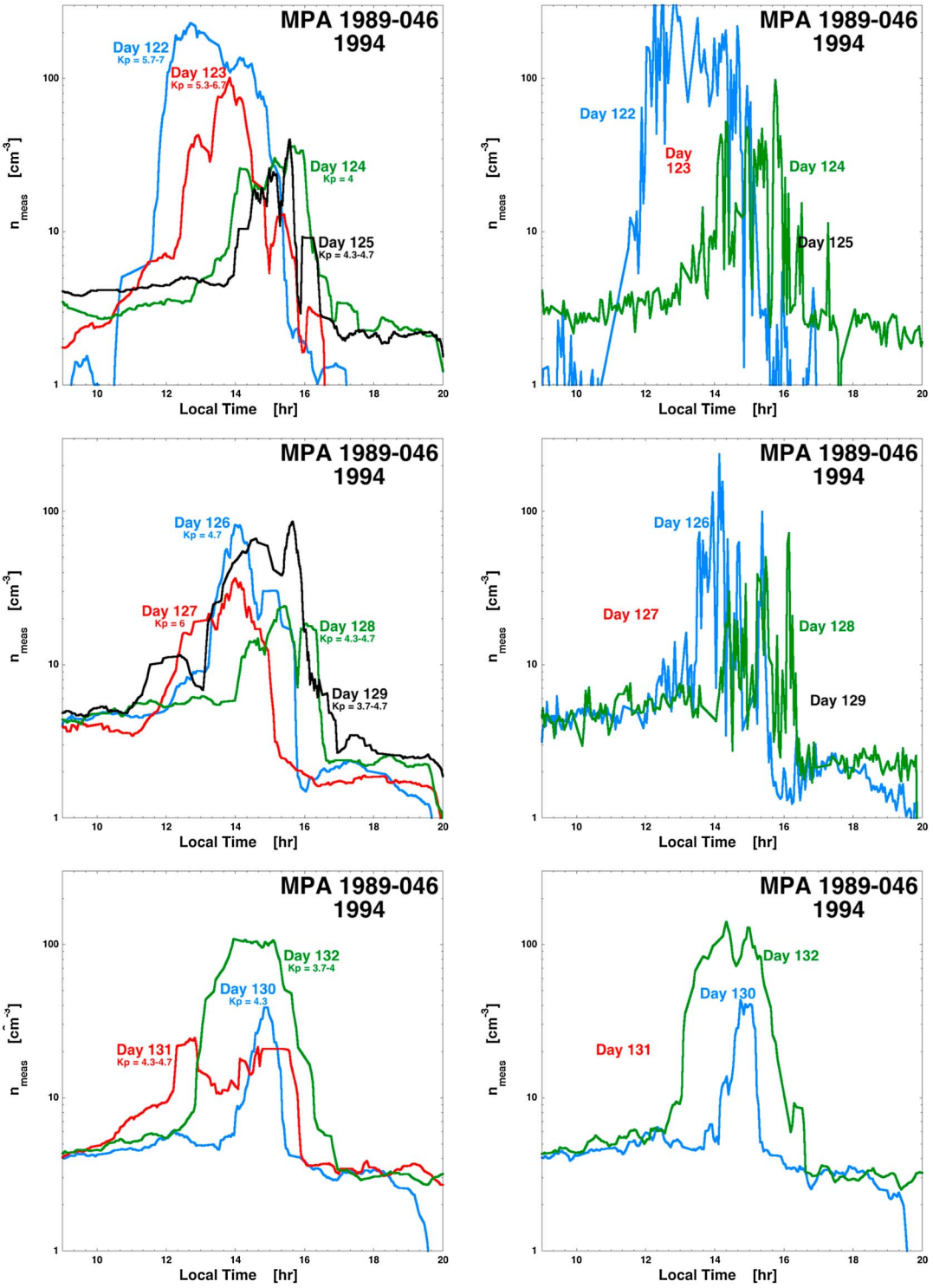

Figure 3. A local time cut each day of the 11 day long plume as seen by MPA. (left) Eleven-point smoothed. (right) Not smoothed.

geosynchronous orbit [e.g., *Sojka and Wrenn*, 1985; *Lawrence et al*., 1998; *Su et al*., 2001a]. This is the filling of the outer plasmasphere during the calm before the storm [*Borovsky and Steinberg*, 2006; *Borovsky and Denton*, 2009a]. During the end of each UT day for Days 121–132, the plasmaspheric plume is crossed by the spacecraft 1989–046 traversing the dayside magnetosphere: this is the brief spike of high-density cold plasma seen in the plot each day. Each daily crossing of the plume is indicated by the number in black on the

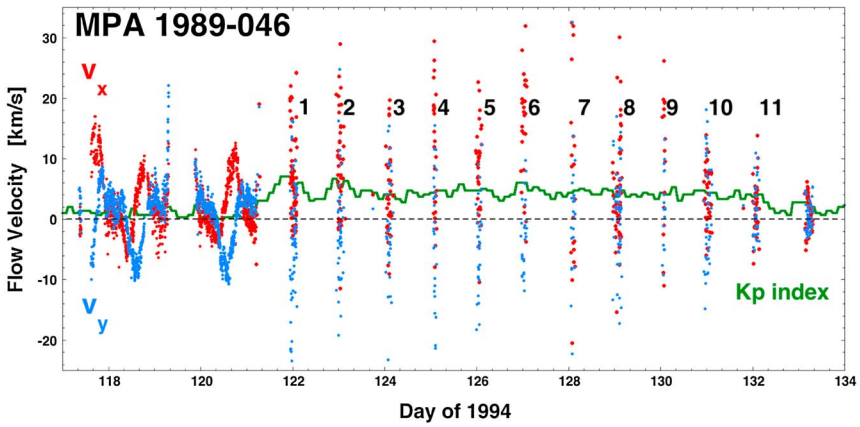

Figure 4. The cold-ion flow velocity measured within the long-lived plasmaspheric plume of Figures 2 and 3 is plotted. The red points are the GSM v_x values, and the blue points are the GSM v_y values. The *Kp* index is plotted in green, and the plume crossing number is indicated in black.

plot. In Figure 2 (bottom) the time at which 1989–046 crosses local noon is marked by an orange dot and the time at which it crosses 18 LT is marked by a black dot. A plasmaspheric plume is expected to lie between local noon and 18 LT [*Borovsky and Denton*, 2008]: these 11 crossings of the plume are in that expected local time range. In this long-duration storm, the plasmaspheric plume is seen for 11 days. In Figure 2 (bottom) cold plasma is seen at the end of Day 132 when geomagnetic activity has subsided, but here it is seen at 18 LT; this is a crossing of the dusk bulge of the plasmasphere [cf. *Chappell et al.*, 1970; *Higel and Wu*, 1984; *Moldwin et al.*, 1994].

Also plotted (logarithmically) as the red curve in Figure 2 (bottom) is the number density of the electron plasma sheet as measured by MPA on board the spacecraft 1989–046 in geosynchronous orbit. Note that the upward spikes of the plasmaspheric density (blue) are colocated with downward dropouts of the hot-electron density (red). The plasmaspheric plume resides in a dayside gap of the electron plasma sheet [cf. *Borovsky et al.*, 2013]. The plasmaspheric plasma in this gap highlights the concept of a plasmaspheric drainage corridor. Note that this electron plasma sheet gap differs from the dayside electron trough [*Thomsen et al.*, 1998], which is a gradual decrease in the hot-electron number density going from the nightside around dawn to the dayside on days with weaker geomagnetic activity. Rather, the gap represents a region from which the warm plasma sheet electron drifts are excluded, i.e., a closed drift zone forbidden to open drift trajectories from the geomagnetic tail.

In Figure 3 the local time profiles of the 11 plume crossings during the May 1994 storm by the spacecraft 1989–046 are shown. Figure 3 (left) plots (logarithmically) the cold-ion number density versus local time for all 11 crossings, and Figure 3 (right) plots the density of every other plume crossing. Figure 3 (right) plots the density with the 86 s time resolution of the MPA instruments, and Figure 3 (left) plots 11 point running averages of the 86 s measurements of the density. An 11-point running average is a 15.8 min running average. During the first day of elevated geomagnetic activity the local time width of the plasmaspheric plume is wider: here in the top panels of Figure 3 it is seen to be about 4 h wide. In the later days it is 2–3 h wide at geosynchronous orbit. The peak number density and the width both fluctuate from crossing to crossing; however, the plume remains robust. Note the crossing of Day 132 (the eleventh day of the plume) in the bottom panels of Figure 3: the plume has a number density at geosynchronous orbit of ~100 cm^{-3}.

Note in Figure 3 (right) that the plume seen with 86 s time resolution is quite lumpy in density. Strong density inhomogeneity seems to be a basic property of plasmaspheric plumes [cf. *Spasojevic et al.*, 2003; *Goldstein et al.*, 2004; *Borovsky and Denton*, 2008; *Matsui et al.*, 2012], and long-lived plumes are no different.

In Figure 4 the cold-ion flow velocity (in GSM coordinates) as measured by MPA on board 1989–046 is plotted before, during, and after the interval of long-lived plasmaspheric plumes. The flow velocity is only plotted if the measured cold-ion number density is above 10 cm^{-3}. Also plotted in green is the *Kp* index. As can be seen, the flow velocity is low on Days 117–120 when the outer plasmasphere is filled; the pattern seen represents the corotation of the outer plasmasphere with deviations caused by the noncircular E × B drift

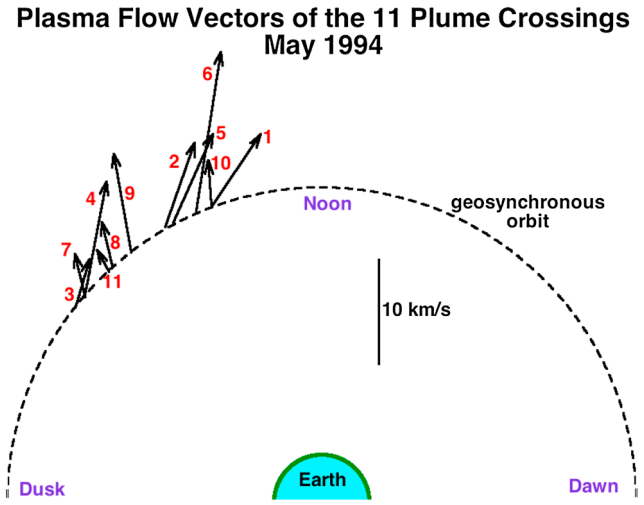

Figure 5. Mean velocity vector for each of 11 plume crossings and the location of the center of the plume along geosynchronous orbit. The plume crossing number (from Figure 4) is indicated in red near each velocity vector.

orbits. The cold-ion flow velocity of the plasmaspheric plume can be seen on Days 121–132 when *Kp* is elevated; in this interval the plume crossing number is marked in black. Note that the flow velocity in the plume fluctuates significantly from measurement to measurement [cf. *Borovsky and Denton*, 2008]. On day 133 where *Kp* is at quiet levels and the plasmaspheric bulge is seen, the cold-ion flow velocity is low with little variability.

In Figure 5 is a sketch of the equatorial plane of the magnetosphere with the mean flow vector for each of the 11 plume crossings of the May 1994 storm laid out with the origin of each vector placed onto geosynchronous orbit where the midpoint of the plume was encountered by 1989–046. The vectors are to scale (see the 10 km/s length indicator on the sketch). The plume (drainage channel) is repeatedly encountered in the postnoon sector, as expected, and the plasma flow is toward the dayside magnetopause. The mean flow speed varies from crossing to crossing and, in general, is strongly correlated with *Kp* at the time of crossing [cf. *Borovsky and Denton*, 2008].

Another example of a long-lived plasmaspheric plume preceded by a calm before the storm appears in Figure 6. This plume occurred in October 2003 when there were six MPA spacecraft operating in geosynchronous orbit, so the temporal continuity of the plume can be monitored. The locations of the six spacecraft carrying MPA plasma instruments are shown in Figure 7, which indicates the local time positions of the six spacecraft at 0 UT. As can be seen, the six spacecraft are spread in longitude. This constellation of spacecraft corotates with the Earth; each day there are six MPA passes across the dayside magnetosphere to monitor the plasmaspheric plume. In Figure 6, 16 days of measurements are plotted. The blue solid curve at

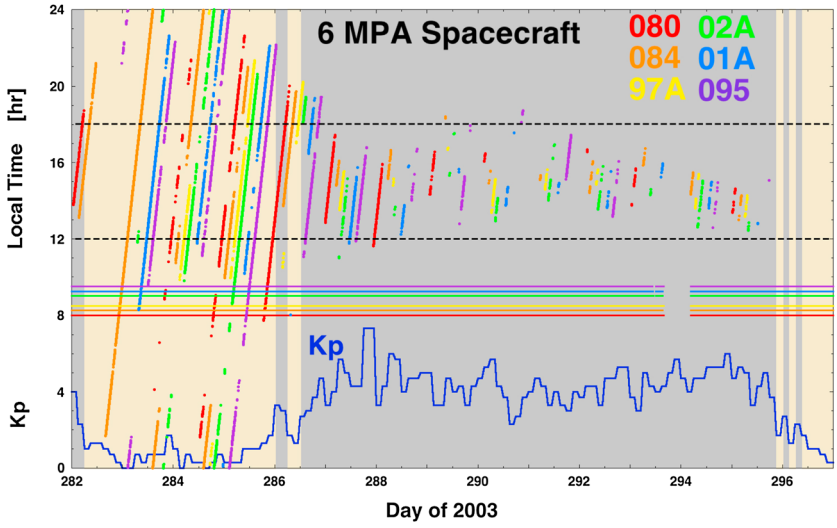

Figure 6. For a long-lived plasmaspheric plume in October 2003, the local times at which six geosynchronous spacecraft measure cold-ion number densities exceeding 20 cm^{-3} are plotted in six colors. At the bottom the *Kp* index is plotted in blue. The horizontal colored curves indicate the availability of MPA data from the six spacecraft.

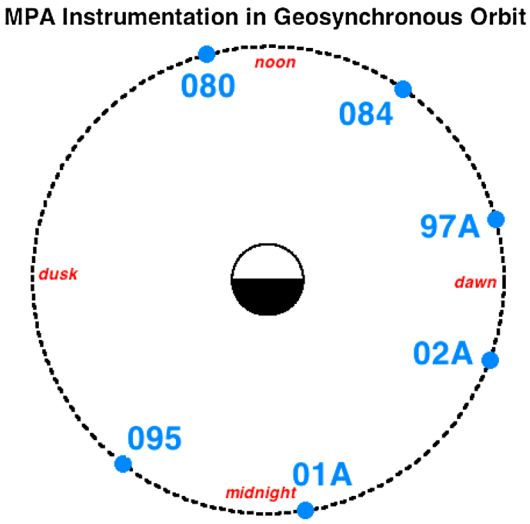

Figure 7. For the long-lived plumes examined in the year 2003, the constellation of six MPA spacecraft in geosynchronous orbit is sketched at 0 UT. The pattern corotates with the Earth.

the bottom of the figure is the *Kp* index. The figure is shaded in gray for times when $Kp > 2$, and it is shaded in brown for times when $Kp \leq 2$. As can be seen, on days 282–285 there is a calm before the storm. On day 286 magnetospheric convection onsets and the *Kp* index rises and remains elevated for 8 days. In the upper portion of Figure 6 the local time positions of the six MPA spacecraft are plotted in six different colors when the cold-ion number density that they measure exceeds 20 cm^{-3}. The two horizontal black dashed lines in the figure indicate 12 LT and 18 LT: a plasmaspheric plume is expected to reside in this range of local times between the two dashed lines. In the middle of Figure 6 the six horizontal curves of different colors indicate the availability of data on the six MPA spacecraft. Note in particular an MPA data gap for all six spacecraft on day 293. During the calm before the storm, plasmaspheric plasma is seen by all six spacecraft at a wide range of local times. This indicates the presence of a filled outer plasmasphere during the calm before the storm. As *Kp* rises on day 286 a broad surge of plasmaspheric plasma is seen across the afternoon sector. In about 1.5 days this narrows into the classic plasmaspheric plume.

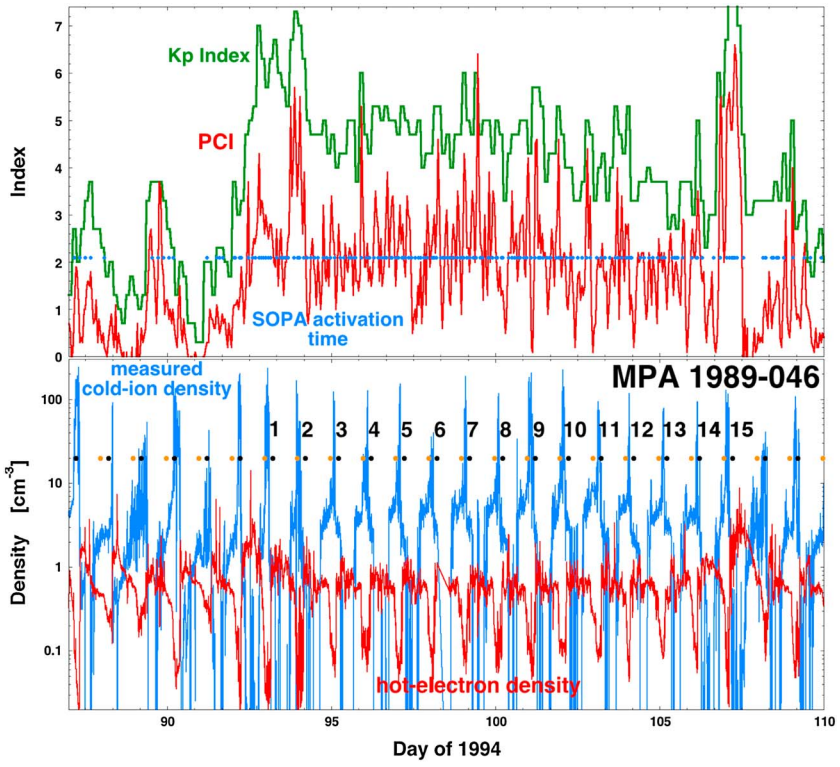

Figure 8. For a long-duration geomagnetic storm in April 1994 that does not have a calm before the storm, a drainage plume lasting 15 days is shown. (top) The *Kp* index (green) and PCI (red) are plotted, and the times of substorm injections are denoted with blue dots. (bottom) The cold-ion density and hot-electron density measured by the spacecraft 1989–046 in geosynchronous orbit are plotted (logarithmically). The times at which 1989–046 crosses local noon are indicated by the orange dots, and the times at which it crosses 18 LT are indicated by the black dots. The plume crossing number is indicated by the black number.

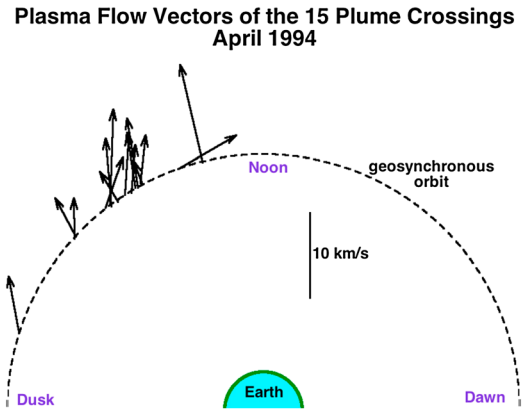

Figure 9. For a storm without a calm before the storm and without a filled outer plasmasphere, the mean velocity vector for each of 15 plume crossings, and the location of the center of the plume along geosynchronous orbit.

As can be seen in the local time plotting in the upper portions of Figure 6, the plume is continually seen by the six spacecraft making their passes across the dayside magnetosphere. Note that when *Kp* drops in magnitude (e.g., on day 290), the position of the plasmaspheric plasma shifts toward dusk.

3. Long-Lived Plasmaspheric Plumes Without a Calm Before the Storm

An example of a long-lived plasmaspheric plume during a storm that does not have a calm before the storm appears in Figure 8. This April 1994 event is from the same equatorward extension of a large southern polar coronal hole [*McAllister et al.*, 1996] as the May 1994 event of Figures 2–5. In Figure 8 (top) the *Kp* index (green) and PCI (red) are plotted as functions of time for 23 days and the times of substorm injections of energetic electrons into geosynchronous orbit are marked with blue dots. In Figure 8 (bottom) the cold-ion number density (blue) and hot-electron number density (red) as measured by the MPA instrument on board 1989–046 in geosynchronous orbit are plotted, with dots marking the times that 1989–046 crosses through local noon (orange) and 18 LT (black). On the Days 87–91 before the storm geomagnetic activity is quiet but not extremely calm; on those days the geosynchronous satellite 1989–046 cuts through the duskside plasmaspheric bulge at about 18 LT each day. For this storm without a well-developed calm before the storm, the plasmasphere is not filled out to geosynchronous orbit at the storm's onset. As *Kp* rises at the beginning of Day 92, a plasmaspheric plume forms, and as *Kp* remains elevated, the plume persists. This plume is seen in the Figure 8 (bottom) as the daily spike of cold-ion density in the dayside magnetosphere between local noon (orange dot) and 18 LT (black dot). The daily plume crossing is numbered in the Figure 8 (bottom); as can be seen the plume persists for 15 days during this long-duration storm.

Since there was not a calm before the storm, there was not a filled outer plasmasphere at the onset of the storm. Hence, the plasmaspheric plume in this case cannot be the drainage of an extended outer plasmasphere, at least not one extended beyond geosynchronous orbit. Note each day in Figure 8 (bottom) the dayside gap in the electron plasma sheet coincident with the position of the plasmaspheric plume.

In the sketch of Figure 9 the mean flow velocity vector for each of the 15 plume crossings are placed onto the locations along geosynchronous orbit where the midpoint of the plume was encountered by 1989–046. During this long-duration storm the long-lived plume is seen for 15 days in the postnoon sector flowing sunward.

A second example of a long-lived plasmaspheric plume that occurs without a calm before the storm is shown in Figure 10; this plume occurred in November 2003 when the six MPA spacecraft were operating in geosynchronous orbit. The format of Figure 10 is the same as the format of Figure 6, and the six-spacecraft constellation appears in Figure 7. The *Kp* index is plotted as the solid blue curve in the bottom of Figure 10 with tan shading for times when $Kp \leq 2$. *Kp* rises on day 313 and remains at sustained levels for 10 days. Prior to day 313 the magnetosphere is alternately calm and active; the local time positions of the spacecraft where they see the cold-ion number density exceeding 20 cm^{-3} indicate that the outer plasmasphere is not filled (compare with Figure 6). Nevertheless, on day 313 when activity has reached high levels a plasmaspheric plume is seen between 12 LT and 18 LT. Throughout days 313–323 the six spacecraft continually see the plasmaspheric plume as they make their passes across the dayside magnetosphere, six crossings per day. Note from the six horizontal colored curves in the middle of Figure 10 that all six spacecraft have MPA data dropouts beginning on day 323.

4. Can the Long-Lived Plumes be Drainage From the Outer Plasmasphere: Advection-Refilling Simulations

To estimate the time that it takes to completely drain the outer plasmasphere (and to get an idea about the effects on plumes of refilling from the ionosphere), computer simulations are run. The Dynamic Global Core

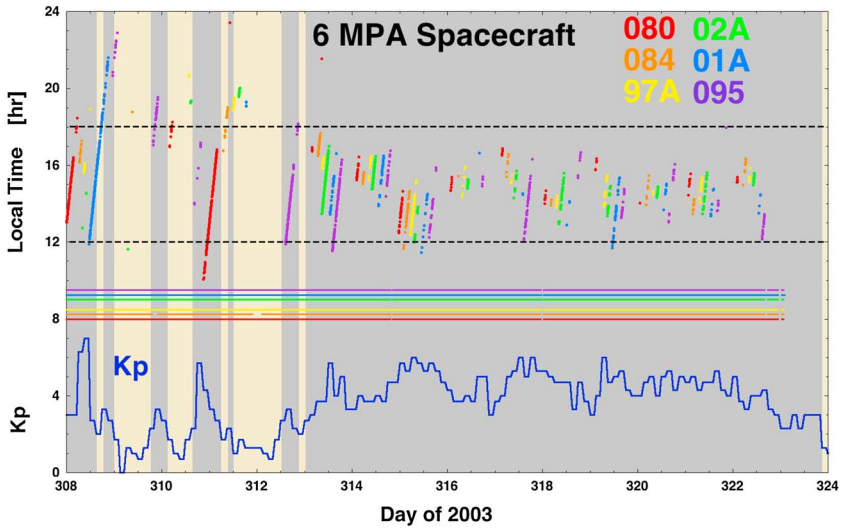

Figure 10. For a long-lived plasmaspheric plume in November 2003, the local times at which six geosynchronous spacecraft measure cold-ion number densities exceeding 20 cm^{-3} are plotted in six colors. At the bottom the *Kp* index is plotted in blue. The horizontal colored curves indicate the availability of MPA data from the six spacecraft.

Plasma Model (DGCPM) is used [*Ober et al*., 1997; *Liemohn*, 2004]. This model advects cold-plasma-filled flux tubes about the Earth using the local E × B drift velocity [*Chen and Wolf*, 1972; *Rasmussen et al*., 1993] in a dipole magnetic field. Equatorial density values are obtained from the volume average of the total flux tube content. The electric field from a variety of sources can be implemented via a coupling of DGCPM with the Space Weather Modeling Framework [*Tóth et al*., 2005; *Dodger and Ridley*, 2014]. For this study, the simple *Kp*-driven Volland-Stern potential model [*Volland*, 1973; *Stern*, 1975] is selected, as it has been shown to be appropriate for capturing storm time plasmasphere dynamics [*Dodger and Ridley*, 2014]. The reader is reminded that, contrary to claims in the literature [e.g., *Pierrard et al*., 2009], these simulations are not MHD simulations: there is no self-consistency associated with the motion of the plasmaspheric plasma (inertial, diamagnetism, or field-aligned currents) nor any feedback on the fields. However, even with their lack of sophistication, such advection models do well at predicting the locations of plasmaspheric boundaries as seen by spacecraft in geosynchronous orbit [e.g., *Lambour et al*., 1997].

Crucial to DGCPM simulations are the ionospheric refilling rate and the atmospheric loss rate, set as a simple source term:

$$\partial N/\partial \mathrm{t} = (N_{\mathrm{sat}} - N(t))/\tau_{\mathrm{fill}} - N(t)/\tau_{\mathrm{loss}}, \quad (1)$$

where $N(t)$ is the time-dependent flux tube content, N_{sat} is the L-dependent saturation content of the flux tube, τ_{fill} is the flux tube refilling time, and τ_{loss} time scale for plasma loss to the atmosphere. The L dependence of N_{sat} is taken from equation (1) of *Carpenter and Anderson* [1992]. The first term on the right-hand side of expression (1) represents dayside refilling to observed quiet time saturation values. While *Rasmussen et al*. [1993] used a refilling constant $\tau_{\mathrm{fill}} = 6.7$ days, this study defaults to a much more aggressive rate of $\tau_{\mathrm{fill}} = 1.5$ days to better match the rapid quiet time refilling rates observed at geosynchronous orbit. The second term on the right-hand side of expression (1) represents nightside losses into the ionosphere. In this study, τ_{loss} is set to 3 days.

To estimate the time scale required to drain the outer plasmasphere, synthetic storm events are simulated wherein *Kp* is set to *Kp* = 1 for 2 days, then elevated to a high level for an additional 5 days. Five simulations are run with five different elevated-*Kp* levels. For these five simulations the plasmaspheric plasma density around geosynchronous orbit is displayed as a local time/universal time map in the five panels of Figure 11: the vertical axis is the local time position around geosynchronous orbit with local noon in the center, and the horizontal axis is time since storm onset in days. The white shading shows the base-10 logarithm of the plasma number density. For all five runs, $\tau_{\mathrm{fill}} = 1.5$ days and $\tau_{\mathrm{loss}} = 3$ days are used. The middle panel of Figure 11 is for *Kp* = 5 during the storm: this *Kp* level is representative of the typical values observed during

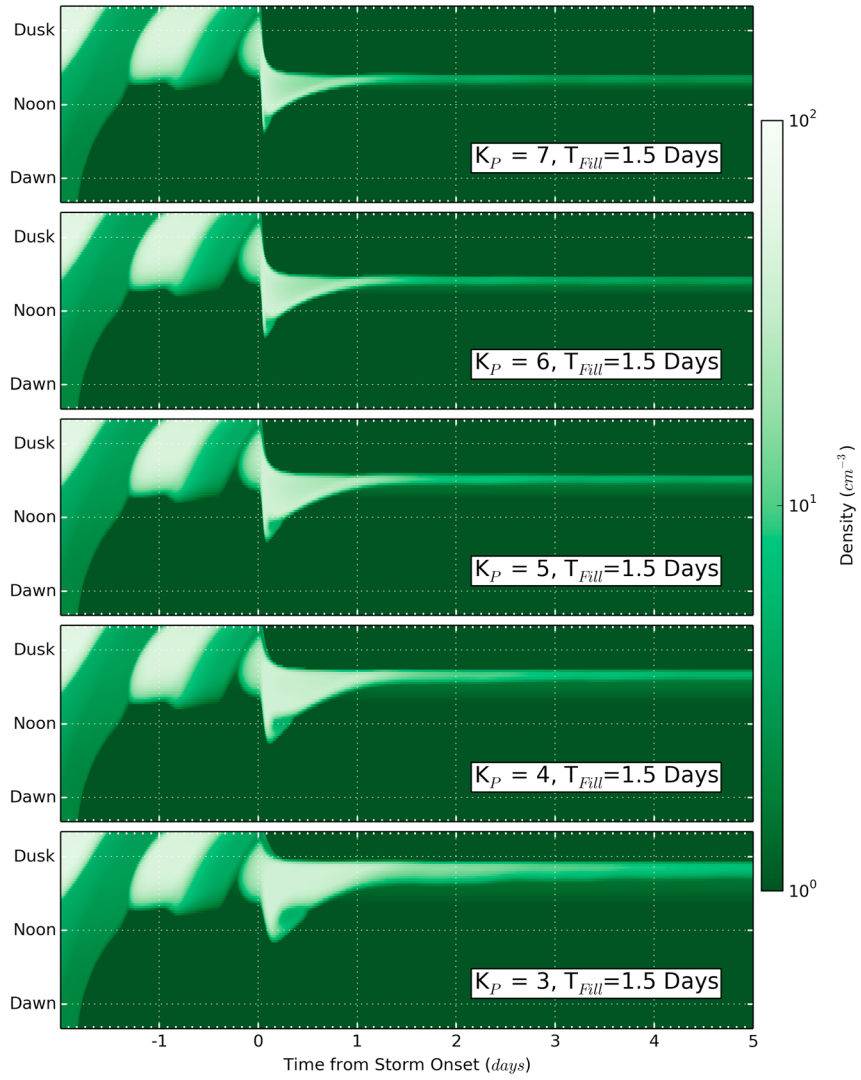

Figure 11. For five simulations with different values of *Kp* after storm onset, the plasmaspheric plasma density around geosynchronous orbit is plotted. Magnetic local time is on the vertical axis such that local noon is in the center, dawn toward the bottom, and dusk toward the top. Time, in days, relative to storm onset is on the horizontal axis.

the actual long-lived plume events. Examining the middle panel, at time $t = 0$, *Kp* is elevated from 1 to 5 and a clear plume develops centered at about 15 LT. During the first 36 h of the storm the filled outer plasmasphere feeds a broad, dense plume (the sunward surge of the outer plasmasphere [*Chen and Wolf*, 1972; *Goldstein*, 2006; *Borovsky et al*., 2013]). This surge decays quickly both in terms of number density and local time width. In the following days, empty flux tubes advect on open drift paths from the nightside to the dayside and begin to accumulate plasma from ionospheric refilling. When the flux tubes join the plume, ionospheric refilling continues to feed plasma into the flux tubes. After 5 days, the plume is still discernable in the simulation, though narrow in local time, and with a very low density.

In the five panels of Figure 11 *Kp* is elevated from $Kp = 1$ before storm onset to five different values after onset: from $Kp = 3$ (bottom frame) to $Kp = 7$ (top frame), in increments of 1. The different storm strengths have several effects on plume development. For higher *Kp* values, the plume shifts toward local noon; for lower *Kp* values, the plume shifts toward dusk. At higher *Kp* the flux tubes that are advecting into the plume originate from lower L shells on the dayside, which means a higher saturation density and therefore a faster refilling rate. This would lead to a stronger mass contribution to the plasmaspheric plume. On the other hand, at higher *Kp*, flux tubes have a shorter travel time before they reach the plume, so less plasma can accumulate.

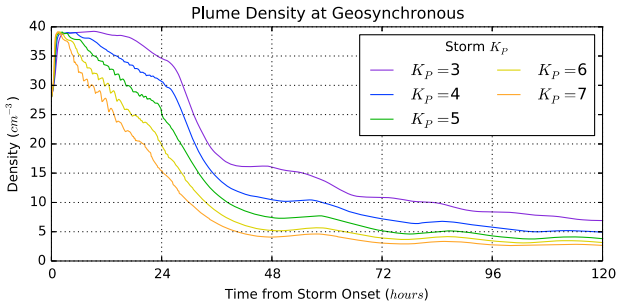

Figure 12. The maximum plasma density in the plume is plotted as a function of time for the five different simulations of Figure 11, each with different storm strengths as designated by the level of *Kp*. Time, in hours, relative to the time of storm onset is shown on the horizontal axis.

This appears to overcome the faster refilling times of lower L shells. The net result is that weaker storms favor denser late time plumes.

Figure 12 plots the maximum density in the plume at geosynchronous orbit as a function of time after storm onset for the five simulations of Figure 11. While the initial density is 40 cm^{-3}, it drops quickly in the first 36 h of the storm: this 36 h is the time required to drain the stored-up outer plasmasphere. With the refilling time set to $\tau_{fill} = 1.5$ days in

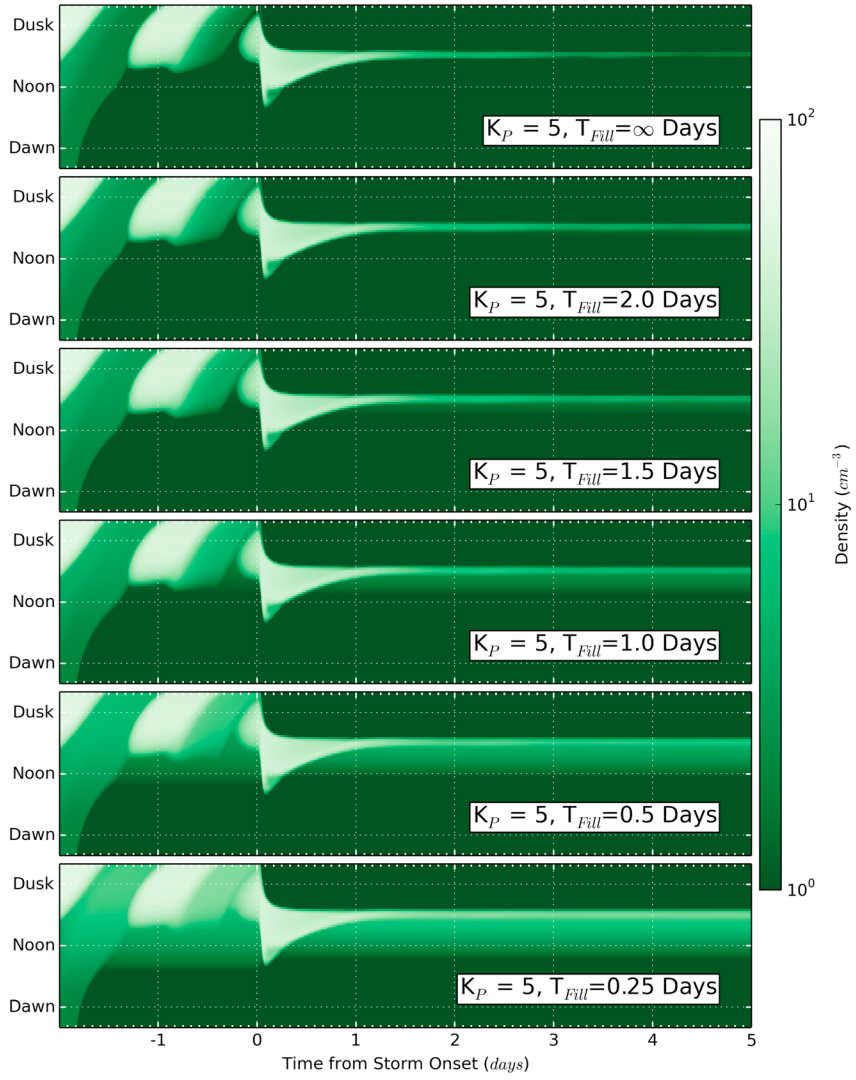

Figure 13. For six simulations with different values of the ionospheric refilling rate, the plasmaspheric plasma density around geosynchronous orbit is plotted. Magnetic local time is on the vertical axis such that local noon is in the center. Time relative to storm onset is on the horizontal axis. The six frames are arranged such that the topmost frame has the slowest refilling rate and the bottom frame has the fastest refilling rate.

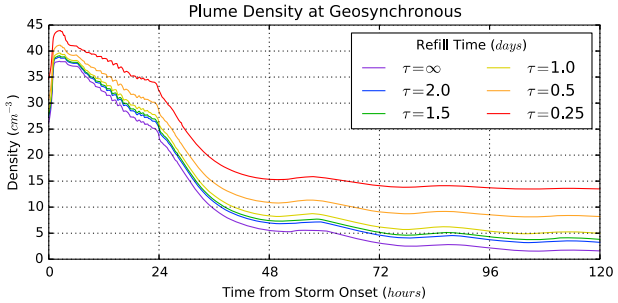

Figure 14. The maximum plasma density in the plume is plotted as a function of time for the six different simulations of Figure 13, each with different ionospheric refilling rates. Time relative to the time of storm onset is shown on the horizontal axis.

the code, the long-lived plumes in the five simulations have number densities in the range of 4–7 cm^{-3}, which is owed to ionospheric outflows into the open drift path flux tubes convecting once through the magnetosphere to join the plume on the dayside. (Note in Figure 12 that the late time plume density in the simulations is larger for *Kp* smaller.) While the model can reproduce the existence and location of long-lived plumes, the model cannot recreate the high densities (~100 cm^{-3}) observed for the long-lived plumes at geosynchronous orbit.

In Figures 13 and 14 a series of six simulations are run for $Kp = 5$ storms with six different values of the ionospheric refilling rate. The refilling rate varies from no refilling ($\tau_{fill} = \infty$), and incrementally from slow ($\tau_{fill} = 2$ days) to fast ($\tau_{fill} = 0.25$ days) refilling rates. Figure 14 shows that with no refilling, the plume decays to negligible density values, dropping to ~5 cm^{-3} in 48 h. As refilling rates are increased, the late time plume becomes denser and more pronounced. As can be seen in the lower panels of Figure 13, dawnward of the plume density peak the plasma density spatially ramps up smoothly as flux tubes are mass loaded from the ionospheric refilling.

Figures 11–14 demonstrate that a filled outer plasmasphere is drained away in about 36–48 h after the onset of the storms. In the simulations, whatever plume remains after 36–48 h is owed to recent ionospheric refilling into the flux tubes advecting sunward in the plume. The long-lived drainage plumes are not fed from plasmaspheric plasma stored in the magnetosphere.

In Figure 15 an interval of the April 1994 event is shown with MPA measurements (black) of the cold-ion density made for nine crossings of the long-lived drainage plume. A simulation with the DGCPM code is run driven by the time-dependent *Kp* of the April 1994 event and with a refilling time $\tau_{fill} = 1.5$ days. The number density in the simulation at the location of the MPA spacecraft is plotted in blue in Figure 15. The location of the peak number density of the plume in the simulation for each crossing is marked with a red vertical line. As can be seen, the simulation predicts the location of the long-lived plume quite accurately but drastically underestimates the number density of the long-lived plume. Note in Figure 15 that the simulation plume is wider than the measured plume; this is undoubtedly owed to numerical diffusion on the computational grid with course spatial resolution. At $L = 6.6$, the azimuthal resolution of the spatial grid is 2200 km.

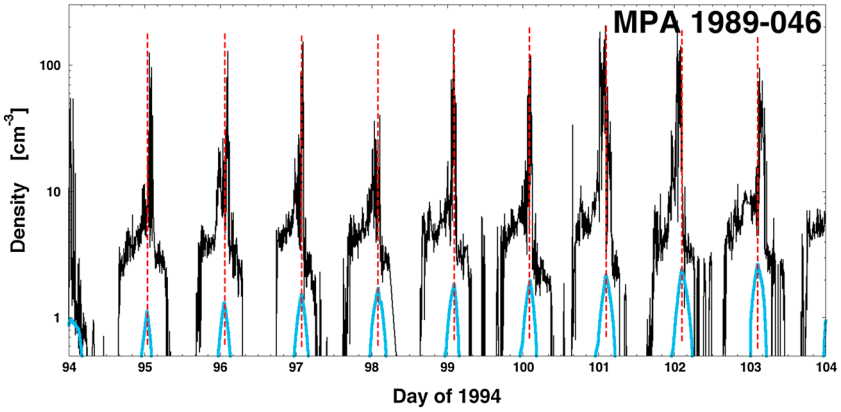

Figure 15. During the long-lived storm of April 1994, the number density of the long-lived drainage plume as measured by the spacecraft 1989–046 is plotted for nine crossing of the plume (black). For a computer simulation of the April 1994 storm using the DGCPM code, the simulated number density of plasmaspheric plasma at the location of 1989–046 is plotted in blue.

Figures 14 and 15 show that even with the fastest refilling rates used here, the model cannot account for the observed high-density values of real-world long-lived plasmaspheric plumes. The maximum plume density for the simulation with the fastest refilling rate is about 15 cm^{-3} (red curve), which is still almost an order of magnitude lower than observations. The results in Figure 14 do imply that ionospheric refilling might be capable of qualitatively creating the observed long-lived-plume signatures, if the refilling rate is strong enough.

5. Potential Sources of the Long-Lived Plasmaspheric Plumes

In sections 5.1, 5.2, and 5.3 three potential sources for the plasma in the long-lived plasmaspheric plumes are briefly explored.

It is taken that the strength of magnetospheric convection does not increase with time during these long-lived storms. If convection was to steadily increase with time, then plasmaspheric plasma from lower and lower L shells could be drained as time progressed, providing a long-lived source of plasma for the plume. The issue of the strength of convection increasing with time is addressed in the Appendix A, with the conclusion that it is not likely that convection is increasing with time.

5.1. Can the Long-Lived Plumes be Diffusing From the Inner Plasmasphere?

A possible source of plasma for the plasmaspheric plume is outward radial diffusion of cold plasma from closed drift paths in the inner plasmasphere onto open drift paths carrying the plasma to the dayside magnetopause [cf. *Matsui et al*., 2000; *Adrian et al*., 2004; see also *Carpenter and Lemaire*, 1997]. To estimate the magnitude of this diffusion, two diffusion coefficients will be calculated: as an upper limit to the rate of diffusion, diffusion by ULF fluctuations will be calculated, and as a lower limit to the rate of diffusion, Bohm diffusion will be calculated.

ULF fluctuating electric fields produce fluctuating E × B drifts that can move particles radially inward and outward. It is well known that this can lead to radial diffusion of energetic particles in the magnetosphere [*Falthammar*, 1965; *Perry et al*., 2005; *Shprits et al*., 2008]; the question is whether it can lead to radial diffusion of cold plasma. For energetic particles which move by a combination of E × B drift and gradient-and-curvature drift, a localized radial perturbation can transport the particles outward by E × B drift wherein they can azimuthally gradient-and-curvature drift out of the perturbation before the localized fluctuation causes particles to E × B drift radially inward. Cold plasma moves with the magnetic field lines, which do not have a net outward transport during the fluctuations. Energetic particles are also subject to violation of adiabatic invariants during ULF fluctuations, whereas cold-plasma particles are not. Hence, radial transport of cold plasma by ULF radial diffusion is probably inefficient. To estimate an absolute upper limit to the spatial diffusion coefficient associated with ULF electric field fluctuations of time scale τ_{ulf}, the diffusion coefficient D_{xx} will be taken to be [*Nicholson*, 1983]

$$D_{xx} \approx \delta x^2 / 2\tau \,, \tag{2}$$

which represents a stepsize δx every time τ. During one period τ_{ulf} of a sinusoidal ULF wave there will be two steps: one in and one out. Hence, the time τ in expression (2) is $\tau = \tau_{ulf}/2$. The stepsize δx is given by an E × B drift of speed $c\delta E/B_o$ of duration $\tau_{ulf}/4$, which is

$$\delta x = (c\delta E/B_o)\ \ \tau_{ulf}/4 \,, \tag{3}$$

where δE is the electric field amplitude of the ULF fluctuations and B_o is the ambient magnetic field strength. Using expression (3) for δx along with $\tau = \tau_{ulf}/2$, expression (2) becomes

$$D_{xx} = c^2 \delta E^2 \tau_{ulf} / 8 {B_o}^2 \,. \tag{4}$$

Using the values of δE as a function of L from the standard deviation curve in Figure 7 of *Matsui et al*. [2003] for $B_z < 0$ (replotted in green in Figure 16), taking B_o for a dipole (plotted in purple in Figure 16), and taking $\tau_{ulf} = 300$ s as typical, the ULF diffusion coefficient for cold plasma is plotted as a function of L in blue in Figure 16.

An important mechanism in plasma physics is Bohm diffusion, which represents diffusion via the disruption of particle gyroorbits. In laboratory experiments, cross-field gradients are often observed to spread at the

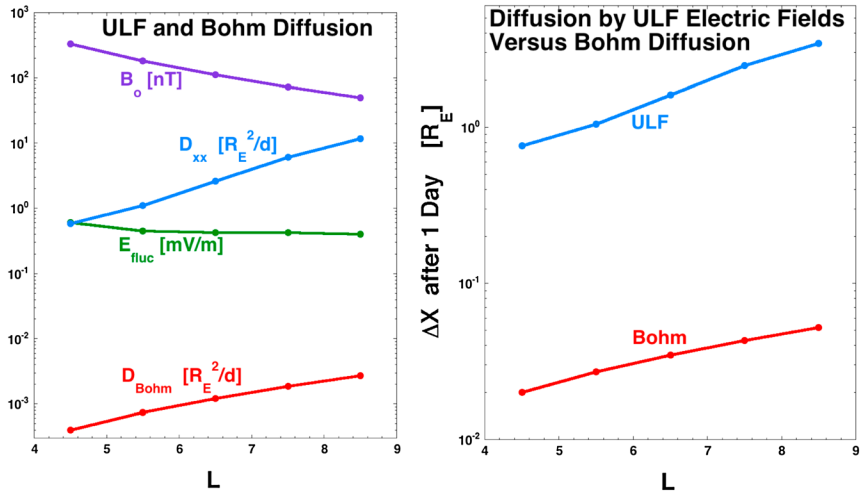

Figure 16. (left) Using ULF electric field for $B_z < 0$ in Figure 7 of *Matsui et al.* [2003], a spatial diffusion coefficient is derived and compared with the coefficient for Bohm diffusion of plasmaspheric plasma. (right) After 1 day of diffusion, the transport distance is plotted for ULF diffusion and Bohm diffusion.

Bohm diffusion rate [*Bohm et al.*, 1949; *Rynn*, 1964]. In various situations the mechanism underlying Bohm diffusion has been attributed to electromagnetic fluctuations [*Lin et al.*, 1980], field line wandering [*Chu et al.*, 1978], stochastic $\underline{E} \times \underline{B}$ drifts [*Taylor and McNamara*, 1971], microturbulent electric fields [*Pecseli and Mikkelsen*, 1985], and drift waves [*Wakatani and Hasegawa*, 1984]. Bohm diffusion acts with a stepsize on the order of a particle gyroradius and a time step on the order of a particle gyroperiod; for a hydrogen plasma with an ion temperature of T_i, the Bohm diffusion coefficient D_B is given by [e.g., *Krall and Trivelpiece*, 1973, equation (1.14.5)]

$$D_B = c\, k_B T_i / 16\, e\, B_o \,. \tag{5}$$

Taking $T_i = 1$ eV for plasmaspheric plasma [*Farrugia et al.*, 1989; *Kutiev et al.*, 2004] and taking B_o to be the dipole field (purple curve in Figure 16), the Bohm diffusion coefficient (expression (5)) for plasmaspheric plasma is plotted as a function of L shell as the red curve in Figure 16. As can be seen, the (lower limit) coefficient for Bohm diffusion is about 3 orders of magnitude smaller than the (upper limit) coefficient for ULF radial diffusion. Note that Coulomb scattering will also produce a (Braginskii) diffusion of plasmaspheric ions across the magnetic field [*Braginskii*, 1965]. For this diffusion, the ion stepsize is the ion gyroradius but the step time is the 90° deflection time τ_d for a thermal ion owing to Coulomb scattering by ions and electrons. Taking $n = 100\,\mathrm{cm}^{-3}$ and $T_i = T_e = 1$ eV, equation (6.4.11) of *Krall and Trivelpiece* [1973] yields $\tau_d = 6.7 \times 10^3$ s = 112 min. At $L = 4$ ($B = 480$ nT), the proton gyroperiod is 0.14 s. Hence, the Braginskii diffusion coefficient for Coulomb scattering is a factor of about $(0.14\,\mathrm{s})/(6.7 \times 10^3\,\mathrm{s}) = 2 \times 10^{-5}$ smaller than the Bohm diffusion coefficient and Coulomb scattering transport can be ignored.

As a gauge of the effectiveness of the diffusion, the spatial transport ΔX by the diffusion in a time t is given by

$$\Delta X = (D\, t)^{1/2} \tag{6}$$

where D is the appropriate diffusion coefficient. Taking D_{xx} from expression (4) for the ULF electric fields of *Matsui et al.* [2003] and taking $t = 1$ day, the value of ΔX for 1 day is plotted as the blue curve in Figure 16 (right). For the ULF upper limit, values of $\Delta X = 1\ R_E$ are found for all L values from 4.5 to 6.5. If the ULF fluctuations were to produce diffusion of the cold plasma, the observed ULF electric field fluctuations are sufficient to produce transport by random motions to distances of ~1 R_E in 1 day. However, it was pointed out above that the ULF radial diffusion of cold plasma is likely to be very inefficient, and so it is likely that the value of $\Delta X = 1\ R_E$ in 1 day is a great overestimation. If this diffusive transport does act on the cold plasma of the plasmasphere, it may contribute to move cold plasma from regions of closed $\mathrm{E} \times \mathrm{B}$ trajectories to regions of open $\mathrm{E} \times \mathrm{B}$ trajectories where the material plume. Taking D_B from expression (5) for Bohm diffusion into expression (6) and taking $t = 1$ day, the value of ΔX for 1 day of Bohm diffusion is plotted as the red curve in Figure 16 (right). For the Bohm diffusion lower limit, values of $\Delta X \sim 0.03\ R_E \sim 200$ km are found for the L values

from 4.5 to 6.5. (See also *Horwitz* [1983] for similar values.) If there is no radial diffusion of cold plasma from the ULF fluctuations, so only Bohm diffusion acts, then the diffusion from the inner magnetosphere to open drift shells will be very small and will not account for the plasma in the plasmaspheric plumes.

5.2. Can the Long-Lived Plumes be Supplied From the Substorm Disruptions of the Plasmapause?

Substorms can disturb and distort the nightside plasmasphere as the fast, short-lived earthward flow from the magnetotail comes into the dipolar portions of the magnetosphere. Azimuthal distortions of the plasmapause are commonly observed [cf. *Moldwin et al*., 1994; *Goldstein et al*., 2002; *Spasojevic et al*., 2003; *Gallagher et al*., 2005; *Darrouzet et al*., 2009]. The simulations of *Spiro et al*. [1981] demonstrated that distortions associated with the occurrence of a substorm can pull "tails" of plasmaspheric plasma out from the nightside plasmasphere onto open drift trajectories wherein this cold plasma convects from the nightside magnetosphere to the dayside magnetopause [see also *Chen and Wolf*, 1972; *Grebowsky and Chen*, 1976].

The following estimate indicates that the substorm disruption of the plasmasphere could move enough plasma out of the plasmasphere to feed the plasmaspheric plume.

At geosynchronous orbit near midnight, the perpendicular (to $\underline{B}$) electric field of a substorm expansion phase is on the order of 5 mV/m westward for a duration of a few minutes [cf. *Shepherd et al*., 1980, Figures 3a and 3b]. For a 100 nT magnetic field at geosynchronous orbit [*Borovsky and Denton*, 2010], this 5 mV/m westward electric field corresponds to a 50 km/s $E \times B$ drift radially toward the Earth: time integrating this 50 km/s drift for a few minutes yields an earthward radial transport of about 1 R_E for $E \times B$ drifting cold plasma at geosynchronous orbit. Away from midnight the substorm expansion phase electric field corresponds to a weaker radially outward convection [*Spiro et al*., 1981; *Birn et al*., 2004; *Birn and Hesse*, 2014; see also *Moore et al*., 2013]. Closer to the Earth than geosynchronous orbit, the radial inward and outward displacements will be smaller. For the purpose of estimation, a 0.5 R_E outward displacement of plasmaspheric plasma at some local times near midnight associated with the occurrence of a substorm is taken. In Figures 2 and 8 the times of substorm injections at geosynchronous orbit are marked as the purple dots. During these two long-lived drainage plumes there are on average 8.6 substorms occurring per day. As the Earth rotates, the plasmaspheric plasma that is on the nightside changes; with approximately eight substorms occurring per day, approximately every longitude of the plasmapause will receive an inward/outward radial displacement of on the order of 0.5 R_E each day.

The *Kp* index is at a level of about 4 during the long-lived plumes of Figures 2 and 8. The *Kp* index and MBI (Midnight Boundary Index) [*Gussenhoven et al*., 1983] are highly correlated, and MBI can be estimated as MBI = 65.27°–1.07 *Kp* [*Borovsky and Denton*, 2009b]. At *Kp* = 4, this gives MBI = 61°. MBI is the magnetic latitude of the inner edge of the electron plasma sheet at local midnight, which is also the magnetic latitude of the plasmapause at local midnight. A dipole latitude of 61° corresponds to $L = 4.25$. In the Gallagher plasmasphere model [*Gallagher et al*., 1995], the plasmaspheric density at $r = 4.25\ R_E$ at local midnight is 370 cm^{-3} (which is equivalent to using the *Carpenter and Anderson* [1992] number density formula $n = 8022\ 10^{-0.3145L}$ for $L = 4.25$). Note that there is a considerable spread in the values of the plasmaspheric number density in the literature: Figure 4 of *Grew et al*. [2007] yields $n = 150$–$2000\ cm^{-3}$ at $L = 4$, whereas Figure 4 of *Darrouzet et al*. [2004] yields $n = 100\ cm^{-3}$ at $L = 4.5$ and Figure 3 of *Decreau et al*. [2005] yields $n = 150\ cm^{-3}$ at $L = 4.5$. These latter two values seem low in light of the fact that the plasmaspheric number density can exceed 100 cm^{-3} at $L = 6.6$ [*Sojka and Wrenn*, 1985; *Su et al*., 2001a]. An annulus in the equatorial plane that is 0.5 R_E wide (from 4.0 R_E to 4.5 R_E) has an area of $5.4 \times 10^{18}\ cm^2$. At $L = 4.25$, a dipole flux tube that has a cross-sectional area in the equatorial plane of 1 cm^2 has a volume of $4.9 \times 10^9\ cm^3$. Hence, the dipole volume of the 0.5 R_E wide annulus is $2.6 \times 10^{28}\ cm^3$. In the Gallagher model at 370 cm^{-3}, the number of plasmaspheric ions in this volume is 9.7×10^{30} ions. If half of these ions are released onto open drift trajectories per day by the nightside substorms hitting the corotating plasmasphere, then the plasmaspheric plume could have a flux of 9.7×10^{30} ions/day (which is 16 t of protons per day).

This estimate of 4.9×10^{30} ions/day corresponds to 5.5×10^{25} ions/s, which falls within the range of plume fluxes measured in the plume survey of *Borovsky and Denton* [2008] (cf. the top panel of Figure 14 of that survey).

This estimate indicates that the perturbation of the nightside plasmasphere by the occurrence of substorms is probably an important contributor to the long-lived plasmaspheric plumes during long-duration storms.

More realistic calculations based on numerical simulations with realistic substorm dynamics [cf. *Birn and Hesse*, 2013, 2014] are needed to better quantify this substorm effect to determine whether or not it is the dominant source of plasma for the long-lived plumes. A further issue to settle is how rapidly the outer layer of the plasmasphere can be refilled from the ionosphere if the substorm transport is depleting it.

Note that smaller-scale flow channels from the magnetotail may also contribute to substorm-like radial transport of plasmaspheric plasma. Undulations of the morningside low-latitude boundary of the diffuse aurora can be seen associated with omega bands [*Jorgensen et al*., 1999; *Kavanagh et al*., 2009; *Henderson*, 2012]. Although there are other suggestions for the cause of omega bands, these undulations may be caused by transient flow bursts in the magnetotail plasma sheet perturbing the inner edge of the electron plasma sheet [cf. *Henderson*, 2012], sort of a minisubstorm perturbation of the dipolar plasma profiles. If the inner edge of the electron plasma sheet is perturbed, then the outer portion of the plasmasphere is also perturbed.

5.3. Can the Long-Lived Plumes be Supplied by Interchange-Type Instabilities?

Interchange-type instabilities have been suggested to give rise to a broadening of the plasmapause [*Richmond*, 1973; *Lemaire*, 1975; *Huang et al*., 1990], which would yield an outward radial transport of plasmaspheric plasma [*Lemaire and Schunk*, 1992; *Dandouras*, 2013]. *Dandouras* [2013] estimate that the quiet time outward radial flux of plasmaspheric protons is as large as the flux in storm time drainage plumes. Interchange instabilities could be driven by the gravity-centripetal drift of plasmaspheric protons building up charge density at the locations of azimuthal (longitudinal) gradients in the plasmaspheric number density [cf. *Newcomb*, 1961] or it could be driven by pressure gradients associated with plasma density gradients [cf. *Southwood and Kivelson*, 1987].

In the equatorial plane, the inner boundary of the electron plasma sheet is proximate to the plasmapause [*Horwitz et al*., 1982; *Elphic et al*., 1999]. The electron plasma sheet is on drift paths originating in the magnetotail and heading to the dayside magnetopause. The plasmasphere near the plasmapause may have a number density ~100 cm^{-3} and a temperature ~1 eV, yielding ~0.02 nPa of particle pressure with an inward pressure gradient at the plasmapause. The electron plasma sheet has a number density ~1 cm^{-3} and a temperature ~2 keV, yielding ~0.3 nPa of particle pressure with an outward pressure gradient near the plasmapause. If the inward pressure gradient of the plasmasphere were to be interchange unstable, it would be stabilized by the proximate and much larger outward pressure gradient of the electron plasma sheet [cf. *Sonnerup and Laird*, 1963]. The pressure gradient of the electron plasma sheet may be sufficient to stabilize a centripetal-driven interchange of the plasmapause [e.g., *Siscoe et al*., 1981]. A further stabilizing outward pressure gradient at the plasmapause would be owed to the warm plasma cloak ions in the electron plasma sheet during active times, with a number density of 2–5 cm^{-3} and a temperature of tens of eV [*Chappell et al*., 2008; *Borovsky et al*., 2013]. All of these particle pressures are dominated at the plasmapause by the ion plasma sheet with a number density ~1 cm^{-3} and a temperature ~20 keV, yielding ~0.3 nPa of pressure. The radial gradient of the ion plasma sheet is gradual and is not focused at the plasmapause. The ion plasma sheet might drive interchange instabilities (which would transport plasmaspheric material radially), but these interchanges would not be driven by or controlled by the plasmasphere. The azimuthal wavelength of any ion-plasma-sheet-driven interchange would be related to the radially broad pressure gradient of the ion plasma sheet. Interchange instabilities may still be driven by the gravity drift of plasmaspheric protons building up charge density at the locations of azimuthal (longitudinal) gradients in the plasmaspheric number density.

Because the inner boundary of the electron plasma sheet is proximate to the plasmapause, the amplitude of interchange instabilities on the plasmapause may be estimated by the amplitude of undulations of the low-latitude boundary of the diffuse aurora. Such undulations are commonly seen during substorms, with larger amplitudes in the dusk regions of local time [*Lui et al*., 1982; *Kelley*, 1986] and smaller amplitudes in the postmidnight regions [*Mendillo et al*., 1989]. The postmidnight event described by *Mendillo et al*. [1989] had an auroral undulation amplitude of 30–60 km in the upper atmosphere, corresponding to 0.1–0.2 R_E in the equatorial plane. This estimated amount of radial transport is smaller than the amount estimated in section 5.1 associated with ULF fluctuations.

Plasmasphere refilling-and-convection models [*Pierrard and Stegun*, 2008; *Pierrard et al*., 2009; *Pierrard and Voiculescu*, 2011] that include the effects of gravitational-centripetal interchange instabilities have been run for April 1994 and the May 1994 long-duration storm events on the European Space Weather

Portal (http://www.spaceweather.eu/en/model_access_interface). In general, the results of the simulations disagree with the observation reported here from geosynchronous orbit. In particular, (1) during the calm before the storm of May 1994 (cf. Figure 2) where the outer plasmasphere fills beyond geosynchronous orbit (6.6 R_E) the European Space Agency Space Weather Portal simulations predict the plasmapause to be located at ~5 R_E in the equatorial plane with no plasmaspheric plasma at 6.6 R_E and (2) during both long-duration storms, even though the code produces an irregular-shaped plasmapause, it does not produce a steady drainage plume, only an occasional (approximately once per day) burst of plasma moving sunward.

The brief analysis of this subsection does not conclude that interchange-driven radial transport can supply the long-lived drainage plumes.

5.4. Can the Long-Lived Plumes be Supplied by Velocity-Shear-Driven Instabilities in the SAPS Region?

It has been argued that velocity-shear-driven instabilities associated with the Sub-Auroral Polarization Stream (SAPS)/subauroral ion drift (SAID) electric field can produce radial displacements of the plasma populations in the duskside magnetosphere in the vicinity of the plasmapause [*Kelley*, 1986; *Yamamoto et al*., 1991, 1994; *Goldstein et al*., 2004; *Henderson et al*., 2010].

The inner edge of the electron plasma sheet is proximate to the plasmapause: if there are radial displacements that are moving the plasmaspheric material, these radial displacements should be visible as undulations of the lower latitude boundary of the diffuse aurora. In the premidnight to afternoon sectors of local time, undulations of the inner edge of the diffuse aurora can have large amplitudes: *Lui et al*. [1982] report amplitudes of 40–400 km in the atmosphere, *Kelley* [1986] report amplitudes of 30–300 km in the atmosphere, and *Biashev et al*. [2010] report amplitudes of 100–150 km in the atmosphere. The smaller of these amplitudes correspond to ~0.1–0.2 R_E radial displacements in the equatorial plane. The largest of these amplitudes could correspond to radial amplitudes of 1–2 R_E in the equatorial plane. Note that the larger of these amplitudes tend to occur at very large values (5–8) of *Kp*, typically beyond the range of *Kp* values seen during long-duration high-speed-stream-driven storms.

For the long-lived high-speed-stream-driven storms that give rise to the long-lived drainage plumes, with *Kp* in the range of 4 to 5, radial displacements of ~0.5 R_E should be common in the duskside magnetosphere. As was the case for the estimate of substorm disruptions of the nightside plasmasphere, the duskside velocity-shear-driven instabilities may be an important mechanism for transporting plasmaspheric plasma radially outward from closed drift trajectories onto open drift trajectories to feed the plume. Again, as was the case for substorm disruptions, a secondary issue would be how rapidly the outwardly transported regions could be refilled from the ionosphere.

5.5. Can the Long-Lived Plumes be the Signature of Anomalous Refilling From the Tongue of Ionization?

Locally in the plasmasphere, the plasmaspheric refilling rate depends on the density of the ionosphere at the magnetic footpoint. In the literature plasmaspheric refilling rates have been measured by observing the temporal filling of the plasmasphere after geomagnetic activity ceases [e.g., *Park*, 1974; *Higel and Wu*, 1984; *Sojka and Wrenn*, 1985; *Lawrence et al*., 1998]. (An exception is *Su et al*. [2001a].) Hence, the refilling rates in the literature correspond to outflow from the ionosphere during quiet times.

During geomagnetically active times enhanced convection brings high-density ionosphere to high latitudes on the dayside; particularly dramatic is the "storm-enhanced density" plume and "tongue of ionization" [*Knudsen*, 1974; *Sojka et al*., 1981; *Foster*, 1993; *Hosokawa et al*., 2010; *Thomas et al*., 2013], which is a high-density region extending from lower latitudes up into the polar cap. With a higher-density ionosphere at high latitudes during geomagnetic activity, the refilling rates for the outer plasmasphere region will be higher than expected during geomagnetically active times. This will be particularly true for the magnetospheric region that magnetically connects to the dayside tongue of ionization. It has been established that the tongue of ionization and the plasmaspheric drainage plume are approximately magnetically connected [*Su et al*., 2001b; *Foster et al*., 2002; *Yizengaw et al*., 2008; *Walsh et al*., 2014].

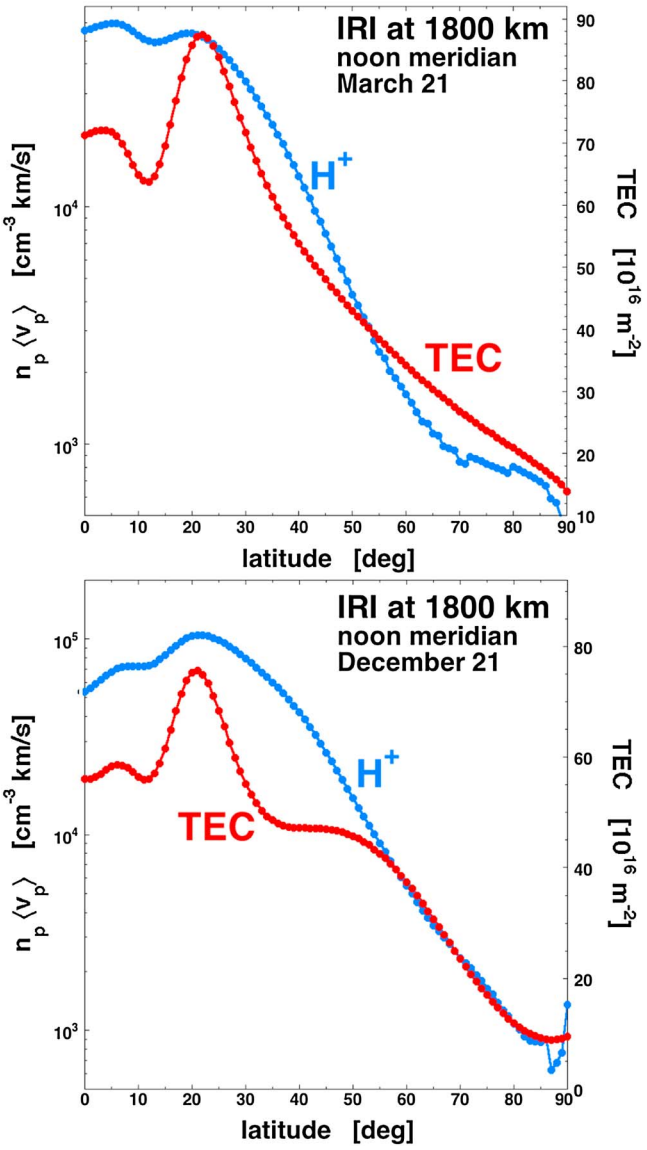

Figure 17. Using the International Reference ionosphere for (top) 21 March 2000 and (bottom) 21 December 2000, the proton number density at 1800 km altitude on the noon meridian (0° longitude) is plotted in blue (left axis) as a function of latitude and the TEC for an altitude up to 2000 km is plotted in red (right axis) for the same meridian as a function of latitude.

Theoretically, the plasmaspheric refilling rate can be estimated from the upward thermal flux of protons in the topside ionosphere; the refilling proton flux F from the ionosphere can be estimated as [cf. *Gombosi*, 1994]

$$F = 0.25\, n_p < v_p > = 0.25\, n_p \left(8 k_B T_p / \Pi m_p\right)^{1/2} \quad (7)$$

where $< v_p >$ is the mean speed of a proton in a population with temperature T_p in the topside ionosphere. Using the International Reference Ionosphere (IRI) [*Lincoln and Conkright*, 1981] to estimate n_p and T_p, the proton flux of expression (7) is calculated at an altitude of 1800 km along the noon meridian: it is plotted (left axis) as a function of latitude as the blue dots in Figure 17 (top) for no dipole tilt (21 March 2000) and in Figure 17 (bottom) for dipole tilt (21 December 2000) in winter. Also plotted in red (right axis) in both panels is the total electron content (TEC) up to 2000 km calculated from IRI.

Examining TEC plots in the literature for the storm time tongue of ionization (e.g., Figure 1 of *Coster et al.* [2007] or Figure 1 of *Walsh et al.* [2014]), at high latitudes the tongue of ionization can produces an increase of TEC by almost a factor of 10 over levels outside the tongue. If the tongue is caused by the convection of more sunlit ionosphere from low latitudes into high latitudes [*Anderson et al.*, 1988; *Sojka et al.*, 1993], then the IRI plots can be used to estimate the increase in topside ion flux F that accompanies the increase in TEC. In Figure 17 (top and bottom), shifting plasma toward higher latitude produces fractional increases in F at higher latitude that are larger than the accompanying fractional increases of TEC. Hence, a factor of 10 increase in F in the tongue of ionization might be reasonable [see also *Hosokawa et al.*, 2010; *Kitanoya et al.*, 2011]. This means that plasmaspheric refilling rates that are a factor of 10 above commonly accepted rates from the literature might also be reasonable.

Refilling rates at geosynchronous orbit (as determined from refilling during quiet times) range from 10 to 50 cm^{-3} d^{-1} [*Sojka and Wrenn*, 1985; *Song et al.*, 1988; *Lawrence et al.*, 1998; *Su et al.*, 2001a] with refilling times of a few days. (Theoretical estimates of the geosynchronous orbit refilling times are somewhat longer than these values [cf. *Rasmussen et al.*, 1993; *Krall and Huba*, 2013].) Boosting these 10–50 cm^{-3} d^{-1} filling

rates by a factor of 10 (to 100–500 cm^{-3} d^{-1}) might be sufficient to supply the observed long-lived plumes from open drift trajectory footpoints that spend a fraction of a day in sunlight.

6. Summary

Long-lived plasmaspheric plumes were found and explored. One plume that was examined lasted for 11 days (Figure 2), and another plume lasted for 15 days (Figure 8).

The long-lived plumes are seen during long-lived high-speed-stream-driven storms. These types of storms typically occur during the declining phase of the solar cycle. Long-lived plumes can occur in storms with calms beforehand and in storms without calms.

It appears to be the case that as long as the *Kp* index remains elevated (i.e., as long as magnetospheric convection is elevated), a plasmaspheric plume can be found.

As seen at geosynchronous orbit, the plume is dense cold (plasmaspheric) plasma advecting sunward in the dayside magnetosphere toward the dayside magnetopause. Cold-plasma number densities from tens to 200 cm^{-3} are seen.

After the initial broad (in local time) surge of cold plasma across the dayside of geosynchronous orbit in the first day of a storm, the plasmaspheric plumes persist for many days and remain robust in number density. The older plumes do not have any characteristics that would distinguish them from younger plumes. They all are lumpy in density, and they reside in a dayside local time gap in the electron plasma sheet.

Magnetospheric-convection simulations indicate that the complete drainage of a builtup outer plasmasphere to the dayside magnetopause should only take 1.5–2 days. After that time, the plasma in the plasmaspheric plumes cannot be simply the drainage of a stored-up outer plasmasphere. Hence, the question arises for long-lived plumes (and for any plume older than about 2 days): Where is the plasma coming from?

Some candidate sources for the plasma in the long-lived plumes were explored. In estimating the amount of plasma that could be supplied to a long-lived drainage plume, three sources are promising.

The first promising candidate for the source of the plasma in long-lived plumes is distortions of the nightside plasmasphere by the occurrence of substorms. Such distortions may result in the outward transport of plasmaspheric material from closed drift orbits onto open drift orbits where the plume can be fed.

The second promising candidate for the source of the plasma in long-lived plumes is the outward transport of plasmaspheric material owed to velocity shear instabilities near the duskside plasmapause.

The third promising candidate for the source of the plasma in long-lived plumes is an anomalously high outflux of cold ionospheric protons from the tongue of ionization in the dayside ionosphere. The tongue of ionization represents anomalously high-density ionospheric plasma that is transported to high latitudes where the ionospheric density is normally low and proton-outflow rates are normally modest.

7. Discussion

The observation in the present study that the long-lived plasmaspheric plumes persist without decreasing in density is contrary to the report [*Borovsky and Denton*, 2008] that plasmaspheric plumes "weaken with age." In the Borovsky-and-Denton survey of plumes, which examined plumes out to an age of 3.5 days in a collection of high-speed-stream-driven storms, it was observed statistically that as the plume age increases the plume width decreases [*Borovsky and Denton*, 2008, Figure 8], the plume density decreases (Figure 10), the plasma flow velocity in the plume decreases (Figure 11), the transported mass flux of the plume decreases (Figure 14), and the local time position of the plume shifts duskward (Figure 8). Part of the statistical result of *Borovsky and Denton* [2008] may be attributable to the transition from the early time plasmaspheric surge during the first day of a storm to the more well developed narrow plume after the first day [cf. *Goldstein*, 2006; *Borovsky et al*., 2013]; at a very early age the surge is wider and denser than the plume at later times [cf. *Borovsky et al*., 2013, Figures 16 and 17]. Another factor in that Borovsky-and-Denton survey was that, statistically, as the plume age increased the *Kp* index decreased; i.e., for that collection of storms *Kp* weakened as the storms progressed. *Kp* is a measure of the strength of convection in the magnetosphere [*Thomsen*, 2004]. A difference between the long-lived plumes explored in the present study and the

collection of plumes surveyed by *Borovsky and Denton* [2008] is that for the long-lived plumes *Kp* is not decreasing, rather it remains at elevated levels in the long-lived storms. It is entirely plausible that the observations of temporal reductions of density, width, flow velocity, and ion flux in the Borovsky-and-Denton survey were caused by the temporal reductions in *Kp*. Note that the local time location of the plumes in that survey [cf. *Borovsky and Denton*, 2008, Figures 8 and 9] also increased toward 18 LT with increasing age: this is a purely *Kp*-dependent property (cf. Figure 11).

8. Work Needed

Work is needed to gain an understanding of where the plasma in the long-lived plasmaspheric plumes is coming from and to be able to predict the properties of these plumes.

If the plume's plasma is coming from the plasmasphere, then a better understanding of the radial transport of plasmaspheric plasma is needed and the question of whether the ionosphere can keep the plasmasphere resupplied for many days needs to be answered. Among other mechanisms, the radial transport may come from velocity-shear-driven instabilities, interchange instabilities, or ULF-driven radial diffusion; these may involve distortions (undulations) of the plasmapause or a broadening of the plasmapause. More work is called for to apply all of these mechanisms to the question of what the source of the long-lived drainage plume is.

If the plume's plasma is not coming from the plasmasphere, then an understanding of how the ionosphere directly supplies this plume is needed. It may be wise to explore mechanisms that can lead to anomalously high refilling rates during geomagnetically active times, such as an enhanced thermal upflux of protons from the tongue of ionization in the high-latitude dayside ionosphere.

Investigation of the disruption of the nightside plasmasphere by the occurrence of substorms is called for. A quantification is needed of how much plasmaspheric material can be transported out to open drift trajectories by the substorm electric fields, along with the refilling rates in the disrupted plasmasphere. Global simulations with realistic substorm dynamics (rapid magnetic reconfiguration with the self-consistent electric fields to support the accompanying flows) are needed.

Clues (or constraints) to what is going on may lie in the facts that (1) the plasmaspheric plume is lumpy (it has great density irregularities) and (2) the plume resides in the narrow dayside gap of the electron plasma sheet. If the plasma in the long-lived plumes is coming from anomalous ionospheric upflows, then there may be a temporal-spatial difference to where cold-H^+ outflow can reach the equatorial plane and where cold-O^+ outflow can reach the equatorial plane.

Appendix A: Could Convection be Strengthening With Time During the Storms?

A key precondition that leads to the dilemma "Where does the plasma come from?" is the assumption that magnetospheric convection does not strengthen with time during these long-lived storms. If the convection is weakening or staying constant, then the plume plasma cannot be coming from deeper and deeper in the inner magnetosphere as time goes on.

This assumption that convection gets weaker with time is based on the *Kp* index, which is one measure of magnetospheric convection [cf. *Thomsen*, 2004].

A more direct measure of the strength of magnetospheric convection is the Midnight Boundary Index (MBI) [*Gussenhoven et al*., 1983; *Madden and Gussenhoven*, 1990], which directly measures the latitude of the equatorward edge of the electron diffuse aurora, which is a measure of how deep into the dipole magnetospheric convection brings the electron plasma sheet. The stronger the convection, the deeper into the dipole and the lower the latitude. In the Figure 18 (top) the *Kp* index is plotted in black for 50 days in the year 1994; these 50 days contain both the April 1994 storm of Figure 8 and the May 1994 storm of Figure 2 which are indicated the two blue arrows in the plot. A 12 h running average of *Kp* is plotted in red. In Figure 18 (middle) MBI is plotted in black for the same 50 days with the two storms indicated by the two blue arrows. A 12 h running average of MBI is plotted in red. When convection increases, the latitude of the edge of the diffuse aurora decreases, so a decrease of MBI in the plot represents an increase of magnetospheric convection. According to MBI (and to *Kp*), the storm in April has convection slowly weakening with time; after and initial very high level of convection on Day 121, the storm in May has convection on average steady with time through the storm.

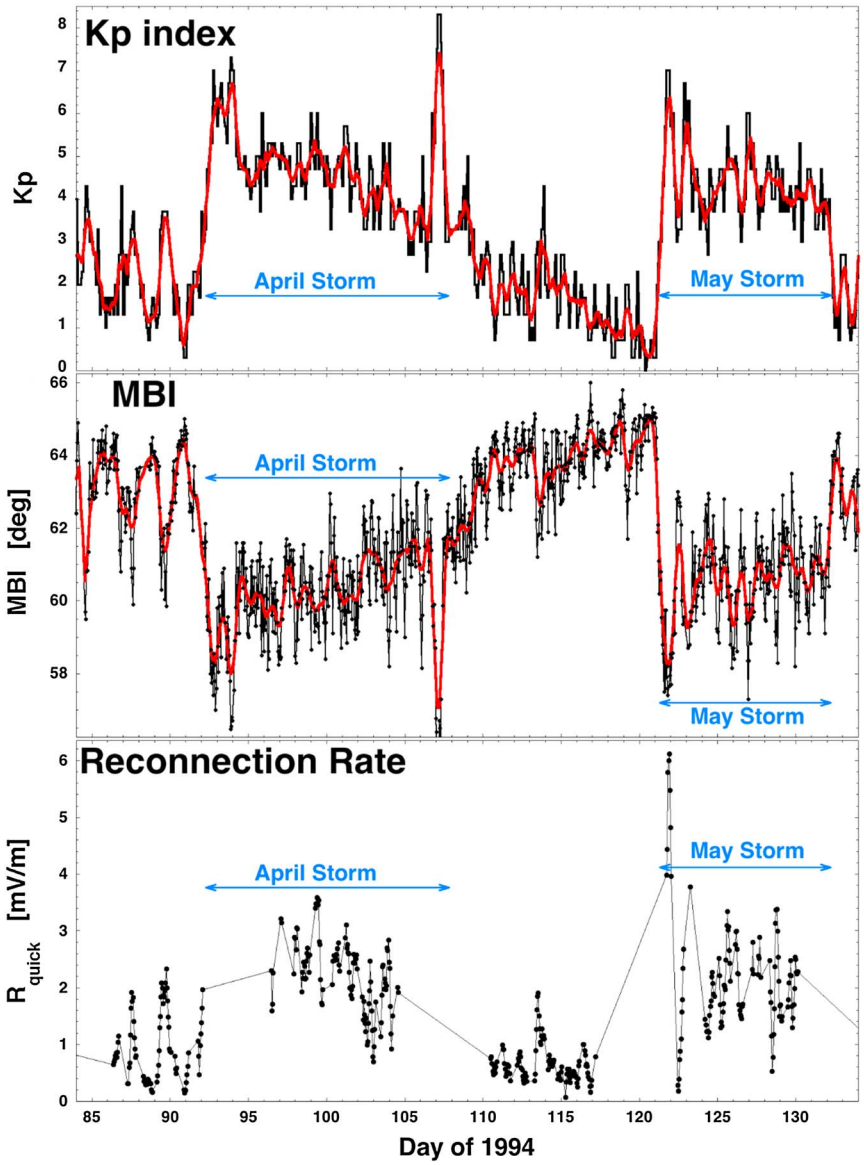

Figure 18. For 50 days in 1994 encompassing the two storms in 1994 with long-lived drainage plumes, (top) the *Kp* index, (middle) the Midnight Boundary Index, and (bottom) the dayside reconnection function R_{quick} are plotted. R_{quick} is only plotted when solar wind measurements are available.

Another gauge of the strength of convection is the strength of reconnection at the dayside magnetosphere. This can be estimated from theoretical calculations of the reconnection rate based on solar wind parameters. One formula is $R_{quick} = 3.89\ \pi^{1/2}\ m_p^{1/2}\ c^{-1}\ n^{1/2} v_{sw}^{2}\ \sin^2(\theta_{clock}/2)\ M_A^{-1.35}\ [1 + 680\ M_A^{-3.30}]^{-1/4}$ [*Borovsky and Birn*, 2014]; here m_p and c are the proton mass and the speed of light and the solar wind parameters are number density (n), speed (v_{sw}), Alfven Mach number (M_A), and IMF clock angle (θ_{clock}). In Figure 18 (bottom) a 5 h running average of the dayside reconnection rate estimate R_{quick} is plotted, where solar wind data are available. Unfortunately, the solar wind data at Earth are sparse in 1994 owing to a lack of satellite coverage. Nevertheless, it can be seen that there is a decline with time of R_{quick} during the portion of the April storm that has solar wind data, and it can be seen that R_{quick} is approximately constant with time during the May storm after the initial high-R_{quick} spike on Day 121.

The conclusion from Figure 18 is that it is unlikely that magnetospheric convection is not increasing with time during these two long-lived storms.

This is probably the case for most high-speed-stream-driven storms since they tend to have a "sawtooth" shape in the temporal plot of *Kp*, with *Kp* rising quickly and then slowly decaying over the duration of the storm. In most cases the decay of *Kp* is probably associated with the trailing edge of the high-speed stream [*Gosling and Pizzo*, 1999; *Burton et al*., 1999] where the solar wind speed declines steadily with time.

Acknowledgments

The authors wish to thank Joachim Birn, Rick Chappell, Jerry Goldstein, Tamas Gombosi, and Mike Henderson for helpful conversations. This work was supported at Space Science Institute by the NSF GEM Program, the NASA CCMSC-24 Program, and the NASA Heliophysics Guest-Investigator Program, at the University of Michigan by the NASA Geospace SR&T Program and at the University of Lancaster by Science and Technology Funding Council grant ST/I000801/1. MPA data are available from NASA CDAWEB at http://cdaweb.gsfc.nasa.gov; simulation outputs are available from Dan Welling at dwelling@umich.edu.

M. Balikhin thanks Charles Chappell and another reviewer for their assistance in evaluating this paper.

References

Adrian, M. L., D. L. Gallagher, and L. A. Avanov (2004), IMAGE EUB observation of radially bifurcated plasmaspheric features: First observations of a possible standing ULF waveform in the inner magnetosphere, *J. Geophys. Res.*, *109*, A01203, doi:10.1029/2003JA009974.

Anderson, D. N., J. Buchau, and R. A. Heelis (1988), Origin of density enhancements in the winter polar cap ionosphere, *Radio Sci.*, *23*, 513, doi:10.1029/RS023i004p00513.

Bame, S. J., D. J. McComas, M. F. Thomsen, B. L. Barraclough, R. C. Elphic, J. P. Glore, J. T. Gosling, J. C. Chavez, E. P. Evans, and F. J. Wymer (1993), Magnetospheric plasma analyzer for spacecraft with constrained resources, *Rev. Sci. Instrum.*, *64*, 1026.

Belian, R. D., G. R. Gisler, T. Cayton, and R. Christensen (1992), High-Z energetic particles at geosynchronous orbit during the great solar proton event series of October 1989, *J. Geophys. Res.*, *97*, 16,897–16,906, doi:10.1029/92JA01139.

Biashev, D. G., E. S. Barkova, A. E. Stepanov, F. Rich, and K. Yumoto (2010), Electric fields and large-scale undulations in the evening sector of the diffuse auroral zone, *Geomagn. Aeron.*, *50*, 41.

Birn, J., and M. Hesse (2013), The substorm current wedge in MHD simulations, *J. Geophys. Res. Space Physics*, *118*, 3364–3376, doi:10.1002/jgra.50187.

Birn, J., and M. Hesse (2014), The substorm current wedge: Further insights from MHD simulations, *J. Geophys. Res. Space Physics*, *119*, 3503–3513, doi:10.1002/2014JA019863.

Birn, J., J. Raeder, Y. L. Wang, R. A. Wolf, and M. Hesse (2004), On the propagation of bubbles in the geomagnetic tail, *Ann. Geophys.*, *22*, 1773–1786.

Bohm, D., E. H. S. Burhop, and H. S. W. Massey (1949), The use of probes for plasma exploration in strong magnetic fields, in *The Characteristics of Electrical Discharges in Magnetic Fields*, edited by A. Guthrie and R. K. Wakerling, p. 13, McGraw-Hill, New York.

Borovsky, J. E. (2014), Feedback of the magnetosphere, *Science*, *343*, 1086–1087.

Borovsky, J. E., and J. Birn (2014), The solar-wind electric field does not control the dayside reconnection rate, *J. Geophys. Res. Space Physics*, *119*, 751–760, doi:10.1002/2013JA019193.

Borovsky, J. E., and M. H. Denton (2006a), The effect of plasmaspheric drainage plumes on solar-wind/magnetosphere coupling, *Geophys. Res. Lett.*, *33*, L20101, doi:10.1029/2006GL026519.

Borovsky, J. E., and M. H. Denton (2006b), The differences between CME-driven storms and CIR-driven storms, *J. Geophys. Res.*, *111*, A07S08, doi:10.1029/2005JA011447.

Borovsky, J. E., and M. H. Denton (2008), A statistical look at plasmaspheric drainage plumes, *J. Geophys. Res.*, *113*, A09221, doi:10.1029/2007JA012994.

Borovsky, J. E., and M. H. Denton (2009a), Electron loss rates from the outer electron radiation belt caused by the filling of the outer plasmasphere: The calm before the storm, *J. Geophys. Res.*, *114*, A11203, doi:10.1029/2009JA014063.

Borovsky, J. E., and M. H. Denton (2009b), Relativistic-electron dropouts and recovery: A superposed-epoch study of the magnetosphere and the solar wind, *J. Geophys. Res.*, *114*, A02201, doi:10.1029/2008JA013128.

Borovsky, J. E., and M. H. Denton (2010), The magnetic field at geosynchronous orbit during high-speed-stream-driven storms: Connections to the solar wind, the plasma sheet, and the outer electron radiation belt, *J. Geophys. Res.*, *115*, A08217, doi:10.1029/2009JA015116.

Borovsky, J. E., and J. T. Steinberg (2006), The "calm before the storm" in CIR/magnetosphere interactions: Occurrence statistics, solar-wind statistics, and magnetospheric preconditioning, *J. Geophys. Res.*, *111*, A07S10, doi:10.1029/2005JA011397.

Borovsky, J. E., M. F. Thomsen, and D. J. McComas (1997), The superdense plasma sheet: Plasmaspheric origin, solar-wind origin, or ionospheric origin?, *J. Geophys. Res.*, *102*, 22,089–22,097, doi:10.1029/96JA02469.

Borovsky, J. E., M. F. Thomsen, D. J. McComas, T. E. Cayton, and D. J. Knipp (1998), Magnetospheric dynamics and mass flow during the November-1993 storm, *J. Geophys. Res.*, *103*(A11), 26,373–26,394, doi:10.1029/97JA03051.

Borovsky, J. E., M. H. Denton, R. E. Denton, V. K. Jordanova, and J. Krall (2013), Estimating the effects of ionospheric plasma on solar-wind/magnetosphere coupling via mass loading of dayside reconnection: Ion-plasma-sheet oxygen, plasmaspheric drainage plumes, and the plasma cloak, *J. Geophys. Res. Space Physics*, *118*, 5695–5719, doi:10.1002/jgra.50527.

Borovsky, J. E., R. H. W. Friedel, and M. H. Denton (2014), Statistically measuring the amount of pitch-angle scattering that energetic electrons undergo as they drift across the plasmaspheric drainage plume at geosynchronous orbit, *J. Geophys. Res. Space Physics*, *119*, 1814–1826, doi:10.1002/2013JA019310.

Bortnik, J., R. M. Thorne, T. P. O'Brien, J. C. Green, R. J. Strangeway, Y. Y. Shprits, and D. N. Baker (2006), Observation of two distinct, rapid loss mechanisms during the 20 November 2003 radiation belt dropout event, *J. Geophys. Res.*, *111*, A12216, doi:10.1029/2006JA011802.

Braginskii, S. I. (1965), Transport processes in a plasma, in *Reviews of Plasma Physics*, vol. 1, edited by M. A. Leontovich, 205 pp., Consultants Bureau, New York.

Burton, M. E., M. Neugebauer, N. U. Crooker, R. von Steiger, and E. J. Smith (1999), Identification of trailing edge solar wind stream interfaces: A comparison of Ulysses plasma and compositional measurements, *J. Geophys. Res.*, *104*, 9925–9932, doi:10.1029/JA104iA05p09925.

Carpenter, D. L., and R. R. Anderson (1992), An ISEE/whistler model of equatorial electron density in the magnetosphere, *J. Geophys. Res.*, *97*, 1097–1108, doi:10.1029/91JA01548.

Carpenter, D. L., and J. Lemaire (1997), Erosion and recovery of the plasmasphere in the plasmapause region, *Space Sci. Rev.*, *80*, 153–179.

Carpenter, D. L., B. L. Giles, C. R. Chappell, P. M. E. Decreau, R. R. Anderson, A. M. Persoon, A. J. Smith, Y. Corcuff, and P. Canu (1993), Plasmasphere dynamics in the duskside bulge region: A new look at an old topic, *J. Geophys. Res.*, *98*, 19,243–19,271, doi:10.1029/93JA00922.

Cayton, T. E., and R. D. Belian (2007), Numerical modeling of the synchronous orbit particle analyzer, Los Alamos National Laboratory Report LA-14335, Los Alamos, N. M.

Chappell, C. R., K. K. Harris, and G. W. Sharp (1970), The morphology of the bulge region of the plasmasphere, *J. Geophys. Res.*, *75*, 3848–3861, doi:10.1029/JA075i019p03848.

Chappell, C. R., K. K. Harris, and G. W. Sharp (1971), The dayside of the plasmapause, *J. Geophys. Res.*, *76*, 7632–7647, doi:10.1029/JA076i031p07632.

Chappell, C. R., M. M. Huddleston, T. E. Moore, B. L. Giles, and D. C. Delcourt (2008), Observations of the warm plasma cloak and an explanation of its formation in the magnetosphere, *J. Geophys. Res.*, *113*, A09206, doi:10.1029/2007JA012945.

Chen, A. J., and R. A. Wolf (1972), Effects on the plasmasphere of a time-varying convection electric field, *Planet. Space Sci.*, *20*, 483–509.
Chu, C., M.-S. Chu, and T. Ohkawa (1978), Magnetostatic mode and cross-field electron transport, *Phys. Rev. Lett.*, *41*, 653.
Coster, A. J., M. J. Colerico, W. Rideout, and F. Rich (2007), Longitude sector comparisons of storm enhanced density, *Geophys. Res. Lett.*, *34*, L18105, doi:10.1029/2007GL030682.
Dandouras, I. (2013), Detection of the plasmaspheric wind in the Earth's magnetosphere by the Cluster spacecraft, *Ann. Geophys.*, *31*, 1143–1153.
Darrouzet, F., et al. (2004), Density structures inside the plasmasphere: Cluster observations, *Ann. Geophys.*, *22*, 2577–2585.
Darrouzet, F., et al. (2009), Plasmaspheric density structures and dynamics: Properties observed by the CLUSTER and IMAGE missions, *Space Sci. Rev.*, *145*, 55–106.
Decreau, P. M. E., E. Le Guirriec, J. L. Rauch, J. G. Trotignon, P. Canu, F. Darrouzet, J. Lemaire, A. Masson, F. Sedgemore, and M. Andre (2005), Density irregularities in the plasmasphere boundary layer: Cluster observations in the dusk sector, *Adv. Space Res.*, *36*, 1964–1969.
Denton, M. H., and J. E. Borovsky (2008), Superposed epoch analysis of high-speed-stream effects at geosynchronous orbit: Hot plasma, cold plasma, and the solar wind, *J. Geophys. Res.*, *113*, A07216, doi:10.1029/2007JA012998.
Dodger, A. M., and A. J. Ridley (2014), Exploring the efficacy of different electric field models in driving a model of the plasmasphere, *J. Geophys. Res. Space Physics*, *119*, 4621–4638, doi:10.1002/2014JA019836.
Elphic, R. C., L. A. Weiss, M. F. Thomsen, D. J. McComas, and M. B. Moldwin (1996), Evolution of plasmaspheric ions at geosynchronous orbit during times of high geomagnetic activity, *Geophys. Res. Lett.*, *23*, 2189-2192, doi:10.1029/96GL02085.
Elphic, R. C., M. F. Thomsen, and J. E. Borovsky (1997), The fate of the outer plasmasphere, *Geophys. Res. Lett.*, *24*, 365–368, doi:10.1029/97GL00141.
Elphic, R. C., M. F. Thomsen, J. E. Borovsky, and D. J. McComas (1999), Inner edge of the electron plasma sheet: Empirical models of boundary location, *J. Geophys. Res.*, *104*(A10), 22,679–22,693, doi:10.1029/1999JA900213.
Falthammar, C.-G. (1965), Effects of time-dependent electric fields on geomagnetically trapped radiation, *J. Geophys. Res.*, *70*, 2503–2516, doi:10.1029/JZ070i011p02503.
Farrugia, C. J., D. T. Young, J. Geiss, and H. Balsiger (1989), The composition, temperature, and density structure of cold ions in the quiet terrestrial plasmasphere: GEOS 1 results, *J. Geophys. Res.*, *94*, 11,865–11,891, doi:10.1029/JA094iA09p11865.
Foster, J. C. (1993), Storm time plasma transport at middle and high latitudes, *J. Geophys. Res.*, *98*, 1675–1689, doi:10.1029/92JA02032.
Foster, J. C., P. J. Erickson, A. J. Coster, J. Goldstein, and F. J. Rich (2002), Ionospheric signatures of plasmaspheric tails, *Geophys. Res. Lett.*, *29*(13), 1623, doi:10.1029/2002GL015067.
Fraser, B. J., T. M. Loto'aniu, and H. J. Singer (2006), Electromagnetic ion cyclotron waves in the magnetosphere, in *Magnetospheric ULF Waves*, *Geophys. Monogr. Ser.*, vol. 169, edited by K. Takahashi et al., p. 195, AGU, Washington, D. C.
Gallagher, D. L., P. D. Craven, R. H. Comfort, and T. E. Moore (1995), On the azimuthal variation of core plasma in the equatorial magnetosphere, *J. Geophys. Res.*, *100*(A12), 23,597–23,605, doi:10.1029/95JA02100.
Gallagher, D. L., M. L. Adrian, and M. W. Liemohn (2005), Origin and evolution of deep plasmaspheric notches, *J. Geophys. Res.*, *110*, A09201, doi:10.1029/2004JA010906.
Goldstein, J. (2006), Plasmasphere response: Tutorial and review of recent imaging results, *Space Sci. Rev.*, *124*, 203–216, doi:10.1007/s11214-006-9105-y.
Goldstein, J., and B. R. Sandel (2005), The global pattern of evolution of plasmaspheric drainage plumes, *Geophys. Monogr.*, *159*, 1.
Goldstein, J., R. W. Spiro, P. H. Reiff, R. A. Wolf, B. R. Sandel, J. W. Freeman, and R. L. Lambour (2002), IMF-driven overshielding electric field and the origin of the plasmaspheric shoulder of May 24, 2000, *Geophys. Res. Lett.*, *29*(16), 1819, doi:10.1029/2001GL014534.
Goldstein, J., B. R. Sandel, M. F. Thomsen, M. Spasojevic, and P. H. Reiff (2004), Simultaneous remote sensing and in situ observations of plasmaspheric drainage plumes, *J. Geophys. Res.*, *109*, A03202, doi:10.1029/2003JA010281.
Gombosi, T. I. (1994), *Gaskinetic Theory*, sect. 7.1.2, Cambridge Univ. Press, New York.
Gosling, J. T., and V. J. Pizzo (1999), Formation and evolution of corotating interaction regions and their three dimensional structure, *Space Sci. Rev.*, *89*, 21–52.
Grebowsky, J. M. (1970), Model study of plasmapause motion, *J. Geophys. Res.*, *75*, 4329–4333, doi:10.1029/JA075i022p04329.
Grebowsky, J. M., and A. J. Chen (1976), Effects on the plasmasphere of irregular electric fields, *Planet. Space Sci.*, *24*, 689.
Grew, R. S., F. W. Menk, M. A. Clilverd, and B. R. Sandel (2007), Mass and electron densities in the inner magnetosphere during a prolonged disturbed interval, *Geophys. Res. Lett.*, *34*, L02108, doi:10.1029/2006GL028254.
Gussenhoven, M. S., D. A. Hardy, and N. Heinemann (1983), Systematics of the equatorward diffuse auroral boundary, *J. Geophys. Res.*, *88*, 5692–5708, doi:10.1029/JA088iA07p05692.
Henderson, M. G. (2012), Auroral substorms, poleward boundary activations, auroral streamers, omega bands and onset precursor activity, in *Auroral Phenomenology and Magnetospheric Processes: Earth And Other Planets*, *Geophys. Monogr. Ser.*, vol. 197, edited by A. Keiling et al., p. 39, AGU, Washington, D. C.
Henderson, M. G., E. F. Donovan, J. C. Foster, I. R. Mann, T. J. Immel, S. B. Mende, and J. B. Sigwarth (2010), Start-to-end global imaging of a sunward propagating SAPS-associated giant undulation event, *J. Geophys. Res.*, *115*, A04210, doi:10.1029/2009JA014106.
Higel, B., and L. Wu (1984), Electron density and plasmapause characteristics at 6.6 Re: A statistical study of GEOS 2 relaxation sounder data, *J. Geophys. Res.*, *89*, 1583–1601, doi:10.1029/JA089iA03p01583.
Horwitz, J. L. (1983), Plasmapause diffusion, *J. Geophys. Res.*, *88*, 4950–4952, doi:10.1029/JA088iA06p04950.
Horwitz, J. L., W. K. Cobb, C. R. Baugher, C. R. Chappell, L. A. Frank, T. E. Eastman, R. R. Anderson, E. G. Shelley, and D. T. Young (1982), On the relationship of the plasmapause to the equatorward boundary of the auroral oval and to the inner edge of the plasma sheet, *J. Geophys. Res.*, *87*, 9059–9069, doi:10.1029/JA087iA11p09059.
Hosokawa, K., T. Tsugawa, K. Shiokawa, Y. Otsuka, N. Nishitani, T. Ogawa, and M. R. Hairston (2010), Dynamic temporal evolution of polar cap tongue of ionization during geomagnetic storms, *J. Geophys. Res.*, *115*, A12333, doi:10.1029/2010JA015848.
Huang, T. S., R. A. Wolf, and T. W. Hill (1990), Interchange instability of the Earth's plasmapause, *J. Geophys. Res.*, *95*, 17,187–17,198, doi:10.1029/JA095iA10p17187.
Jordanova, V. K., M. Spasojevic, and M. F. Thomsen (2007), Modeling the electromagnetic ion cyclotron wave-induced formation of detached subauroral proton arcs, *J. Geophys. Res.*, *112*, A08209, doi:10.1029/2006JA012215.
Jorgensen, A. M., H. E. Spence, T. J. Hughes, and D. McDiarmid (1999), A study of omega bands and Ps6 pulsations on the ground, at low altitude and at geostationary orbit, *J. Geophys. Res.*, *104*, 14,705–14,715, doi:10.1029/1998JA900100.
Kavanagh, A. J., J. A. Wild, and F. Honary (2009), Observations of omega bands using an imaging riometer, *Ann. Geophys.*, *27*, 4183–4195.
Kelley, M. C. (1986), Intense sheared flow as the origin of large-scale undulations of the edge of the diffuse aurora, *J. Geophys. Res.*, *91*, 3225–3230, doi:10.1029/JA091iA03p03225.
Kitanoya, Y., T. Abe, A. W. Yau, T. Hori, and N. Nishitani (2011), Localized electron density enhancements in the high-altitude polar ionosphere and their relationships with storm-enhanced density (SED) plumes and polar tongues of ionization (TOI), *Ann. Geophys.*, *29*, 367–375.

Knudsen, W. C. (1974), Magnetospheric convection and the high-latitude F_2 ionosphere, *J. Geophys. Res.*, *79*, 1046–1055, doi:10.1029/JA079i007p01046.
Krall, J., and J. D. Huba (2013), SAMI3 simulation of plasmasphere refilling, *Geophys. Res. Lett.*, *40*, 2484–2488, doi:10.1002/grl.50458.
Krall, N. A., and A. W. Trivelpiece (1973), *Principles of Plasma Physics*, McGraw-Hill, New York.
Kutiev, I., K.-I. Oyama, S. Watanabe, T. Abe, and A. Kumamoto (2004), Plasmasphere electron temperature structures, *Adv. Space Res.*, *34*, 2010–2015.
Lambour, R. L., L. A. Weiss, R. C. Elphic, and M. F. Thomsen (1997), Global modeling of the plasmasphere following sudden commencements, *J. Geophys. Res.*, *102*(A11), 24,351–24,368, doi:10.1029/97JA02037.
Lawrence, D. J., M. F. Thomsen, J. E. Borovsky, and D. J. McComas (1998), Measurements of early and late-time plasmasphere refilling as observed from geosynchronous orbit, *J. Geophys. Res.*, *104*, 14,691–14,704, doi:10.1029/1998JA900087.
Lemaire, J. (1975), Mechanisms of formation of plasmapause, *Ann. Geophys.*, *31*, 175–190.
Lemaire, J., and R. W. Schunk (1992), Plasmaspheric wind, *J. Atmos. Sol. Terr. Phys.*, *54*, 467–477.
Liemohn, M. W. (2004), Dependence of plasmaspheric morphology on the electric field description during the recovery phase of the 17 April 2002 magnetic storm, *J. Geophys. Res.*, *109*, A03209, doi:10.1029/2003JA010304.
Lin, A. T., J. M. Dawson, and H. Okuda (1980), Cross-field electron transport due to thermal electromagnetic fluctuations, *Phys. Fluids*, *23*, 1316.
Lincoln, J. V., and R. O. Conkright (1981), *International Reference Ionosphere—IRI 79*, World Data Center A, Boulder, Colo.
Lui, A. T. Y., C.-I. Meng, and S. Ismail (1982), Large amplitude undulations on the equatorward boundary of the diffuse aurora, *J. Geophys. Res.*, *87*, 2385–2400, doi:10.1029/JA087iA04p02385.
Madden, D., and M. S. Gussenhoven (1990), Auroral Boundary Index from 1983 to 1990, *Tech Report GL-TR-90-0358,* Air Force Geophysics Laboratory, Hanscom AFB, Mass.
Matsui, H., T. Mukai, S. Ohtani, K. Hayashi, R. C. Elphic, M. F. Thomsen, and H. Matsumoto (1999), Cold dense plasma in the outer magnetosphere, *J. Geophys. Res.*, *104*, 25,077–25,095, doi:10.1029/1999JA900046.
Matsui, H., M. Nakamura, T. Terasawa, Y. Izaki, T. Mukai, K. Tsuruda, H. Hayakawa, and H. Matsumoto (2000), Outflow of cold dense plasma associated with variation of convection in the outer magnetosphere, *J. Atmos. Sol. Terr. Phys.*, *62*, 521–526.
Matsui, H., J. M. Quinn, R. B. Torbert, V. K. Jordanova, W. Baumjohann, P. A. Puhl-Quinn, and G. Paschmann (2003), Electric field measurements in the inner magnetosphere by Cluster EDI, *J. Geophys. Res.*, *108*(A9), 1352, doi:10.1029/2003JA009913.
Matsui, H., F. Darrouzet, J. Goldstein, P. A. Puhl-Quinn, Y. V. Khotyaintsev, P.-A. Lindqvist, E. Georgescu, C. G. Mouikis, and R. B. Torbert (2012), Multi-spacecraft observations of small-scale fluctuations in density and fields in plasmaspheric plumes, *Ann. Geophys.*, *30*, 623.
McAllister, A. H., M. Dryer, P. McIntosh, H. Singer, and L. Weiss (1996), A large polar crown coronal mass ejection and a "problem" geomagnetic storms: April 14–23, 1994, *J. Geophys. Res.*, *101*, 13,497–13,515, doi:10.1029/96JA00510.
McFadden, J. P., C. W. Carlson, D. Larson, J. Bonnell, F. S. Mozer, V. Angelopoulos, K.-H. Glassmeier, and U. Auster (2008), Structure of plasmaspheric plumes and their participation in magnetopause reconnection: First results from THEMIS, *Geophys. Res. Lett.*, *35*, L17S10, doi:10.1029/2008GL033677.
McPherron, R. L., D. N. Baker, and N. U. Crooker (2009), Role of the Russell-McPherron effect in the acceleration of relativistic electrons, *J. Atmos. Sol. Terr. Phys.*, *71*, 1032–1044.
Mendillo, M., J. Baumgardner, and J. Providakes (1989), Ground-based imaging of detached arcs, ripples in the diffuse aurora, and patches of 6300-Å emission, *J. Geophys. Res.*, *94*, 5367–5381, doi:10.1029/JA094iA05p05367.
Millan, R. M., and R. M. Thorne (2007), Review of radiation belt relativistic electron losses, *J. Atmos. Sol. Terr. Phys.*, *69*, 362.
Moldwin, M. B., M. F. Thomsen, S. J. Bame, D. J. McComas, and K. R. Moore (1994), An examination of the structure and dynamics of the outer plasmasphere using multiple geosynchronous satellites, *J. Geophys. Res.*, *99*, 11,475–11,481, doi:10.1029/93JA03526.
Moore, T. E., M. O. Chandler, N. Buzulukova, G. A. Collinson, E. L. Kepko, K. S. Garcia-Sage, M. G. Henderson, and M. I. Sitnov (2013), "Snowplow" injection ion fronts, *J. Geophys. Res. Space Physics*, *118*, 6478–6488, doi:10.1002/jgra.50573.
Newcomb, W. A. (1961), Convective instability induced by gravity in a plasma with a frozen-in magnetic field, *Phys. Fluids*, *4*, 391–396.
Nicholson, D. R. (1983), *Introduction to Plasma Theory, Appendix B*, John Wiley, New York.
Ober, D. M., J. L. Horwitz, and D. L. Gallagher (1997), Formation of density troughs embedded in the outer plasmasphere by subauroral ion drifts, *J. Geophys. Res.*, *102*, 14,595–14,602, doi:10.1029/97JA01046.
Park, C. G. (1974), Some features of plasma distribution in the plasmasphere deduced from Antarctic whistlers, *J. Geophys. Res.*, *79*, 169, doi:10.1029/JA079i001p00169.
Pecseli, H. L., and T. Mikkelsen (1985), Turbulent diffusion in two-dimensional, strongly magnetized plasmas, *J. Plasma Phys.*, *34*, 77–94.
Perry, K. L., M. K. Hudson, and S. R. Elkington (2005), Incorporating spectral characteristics of Pc5 waves into three-dimensional radiation belt modeling and the diffusion of relativistic electrons, *J. Geophys. Res.*, *110*, A03215, doi:10.1029/2004JA010760.
Pierrard, V., and K. Stegun (2008), A three-dimensional dynamic kinetic model of the plasmasphere, *J. Geophys. Res.*, *113*, A10209, doi:10.1029/2008JA013060.
Pierrard, V., and M. Voiculescu (2011), The 3D model of the plasmasphere coupled to the ionosphere, *Geophys. Res. Lett.*, *38*, L12104, doi:10.1029/2011GL047767.
Pierrard, V., J. Goldstein, N. Andre, V. K. Jordanova, G. A. Kotova, J. F. Lemaire, M. W. Liemohn, and H. Matsui (2009), Recent progress in physics-based models of the plasmasphere, *Space Sci. Rev.*, *145*, 193.
Rasmussen, C. E., S. M. Guiter, and S. G. Thomas (1993), A two-dimensional model of the plasmasphere: Refilling time constants, *Planet. Space Sci.*, *41*, 25.
Richmond, A. D. (1973), Self-induced motions of thermal plasma in the magnetosphere and the stability of the plasmapause, *Radio Sci.*, *8*, 1019–1027, doi:10.1029/RS008i011p01019.
Rynn, N. (1964), Classical and enhanced diffusion in cesium and potassium plasmas, *Phys. Fluids*, *7*, 1084.
Sandel, B. R., and M. H. Denton (2007), Global view of refilling of the plasmasphere, *Geophys. Res. Lett.*, *34*, L17102, doi:10.1029/2007GL030669.
Shepherd, G. G., R. Bostrom, H. Derblom, C.-G. Falthammar, R. Gendrin, K. Kaila, A. Korth, A. Pedersen, R. Pellinen, and G. Wrenn (1980), Plasma and field signatures of poleward propagating auroral precipitation observed at the foot of the Geos 2 field line, *J. Geophys. Res.*, *85*, 4587–4601, doi:10.1029/JA085iA09p04587.
Shprits, Y. Y., S. R. Elkington, N. P. Meredith, and D. A. Subbotin (2008), Review of modeling of losses and sources of relativistic electrons in the outer radiation belt I: Radial transport, *J. Atmos. Sol. Terr. Phys.*, *70*, 1679.
Siscoe, G. L., A. Eviatar, R. M. Thorne, J. D. Richardson, F. Bagenal, and J. D. Sullivan (1981), Ring current impoundment of the Io plasma torus, *J. Geophys. Res.*, *86*, 8480–8484, doi:10.1029/JA086iA10p08480.
Sojka, J. J., and G. L. Wrenn (1985), Refilling of geosynchronous flux tubes as observed at the equator by GEOS 2, *J. Geophys. Res.*, *90*, 6379–6385, doi:10.1029/JA090iA07p06379.

Sojka, J. J., W. J. Raitt, and R. W. Schunk (1981), Density features associated with strong convection in the winter high-latitude F region, *J. Geophys. Res.*, *86*, 6968–6976.
Sojka, J. J., M. D. Bowline, R. W. Schunk, D. T. Decker, C. E. Valladares, R. Sheehan, D. N. Anderson, and R. A. Heelis (1993), Polar cap F-region patches using time varying convection, *Geophys. Res. Lett.*, *20*, 1783–1786, doi:10.1029/93GL01347.
Song, X.-T., R. Gendrin, and G. Caudal (1988), Refilling process in the plasmasphere and its relation to magnetic activity, *J. Atmos. Sol. Terr. Phys.*, *50*, 185–195.
Sonnerup, B. U. O., and M. J. Laird (1963), On magnetospheric interchange instability, *J. Geophys. Res.*, *68*, 131–139, doi:10.1029/JZ068i001p00131.
Southwood, D. J., and M. G. Kivelson (1987), Magnetospheric interchange instability, *J. Geophys. Res.*, *92*, 109–116, doi:10.1029/JA092iA01p00109.
Spasojevic, M., J. Goldstein, D. L. Carpenter, U. S. Inan, B. R. Sandel, M. B. Moldwin, and B. W. Reinisch (2003), Global response of the plasmasphere to a geomagnetic disturbance, *J. Geophys. Res.*, *108*(A9), 1340, doi:10.1029/2003JA009987.
Spasojevic, M., H. U. Frey, M. F. Thomsen, S. A. Fuselier, S. P. Gary, B. R. Sandel, and U. S. Inan (2004), The link between a detached subauroral proton arc and a plasmaspheric plume, *Geophys. Res. Lett.*, *31*, L04803, doi:10.1029/2010GL042711.
Spiro, R. W., M. Harel, R. A. Wolf, and P. H. Reiff (1981), Quantitative simulation of a magnetospheric substorm 3. Plasmaspheric electric fields and evolution of the plasmapause, *J. Geophys. Res.*, *86*, 2261–2272, doi:10.1029/JA086iA04p02261.
Stern, D. P. (1975), The motion of a proton in the equatorial magnetosphere, *J. Geophys. Res.*, *80*, 595–599, doi:10.1029/JA080i004p00595.
Su, Y.-J., J. E. Borovsky, M. F. Thomsen, R. C. Elphic, and D. J. McComas (2000), Plasmaspheric material at the reconnecting magnetopause, *J. Geophys. Res.*, *105*, 7591–7600, doi:10.1029/1999JA000266.
Su, Y.-J., M. F. Thomsen, J. E. Borovsky, and D. J. Lawrence (2001a), A comprehensive survey of plasmasphere refilling at geosynchronous orbit, *J. Geophys. Res.*, *106*, 25,615–25,629, doi:10.1029/2000JA000441.
Su, Y.-J., M. F. Thomsen, J. E. Borovsky, and J. C. Foster (2001b), A linkage between polar patches and plasmaspheric drainage plumes, *Geophys. Res. Lett.*, *28*, 111–113, doi:10.1029/2000GL012042.
Taylor, J. B., and B. McNamara (1971), Plasma diffusion in two dimensions, *Phys. Fluids*, *14*, 1492–1499.
Thomas, E. G., J. B. H. Baker, J. M. Ruohoniemi, L. B. N. Clausen, A. J. Coster, J. C. Foster, and P. J. Erickson (2013), Direct observation of the role of convective electric field in the formation of a polar tongue of ionization from storm enhanced density, *J. Geophys. Res. Space Physics*, *118*, 1180–1189, doi:10.1002/jgra.50116.
Thomsen, M. F. (2004), Why Kp is such a good measure of magnetospheric convection, *Space Weather*, *2*, S11044, doi.10.1029/2004SW000089.
Thomsen, M. F., D. J. McComas, J. E. Borovsky, and R. C. Elphic (1998), The magnetospheric trough, in *Geospace Mass and Energy Flow*, *Geophys. Monogr. Ser.*, vol. 104, edited by J. L. Horwitz, D. L. Gallagher, and W. K. Peterson, p. 355, AGU, Washington, D. C.
Thomsen, M. F., E. Noveroske, J. E. Borovsky, and D. J. McComas (1999), Calculating the moments from measurements by the Los Alamos Magnetospheric Plasma Analyzer, LA-13566-MS, Los Alamos National Laboratory, Los Alamos, N. M.
Tóth, G., et al. (2005), Space weather modeling framework: A new tool for the space science community, *J. Geophys. Res.*, *110*, A12226, doi:10.1029/2005JA011126.
Volland, H. (1973), A semiempirical model of large-scale magnetospheric electric fields, *J. Geophys. Res.*, *78*, 171–180, doi:10.1029/JA078i001p00171.
Wakatani, M., and A. Hasegawa (1984), A collisional drift wave description of plasma edge turbulence, *Phys. Fluids*, *27*, 611.
Walsh, B. M., D. G. Sibeck, Y. Nishimura, and V. Angelopoulos (2013), Statistical analysis of the plasmaspheric plume at the magnetopause, *J. Geophys. Res. Space Physics*, *118*, 4844–4851, doi:10.1002/jgra.50458.
Walsh, B. M., J. C. Foster, P. J. Erickson, and D. G. Sibeck (2014), Simultaneous ground and space-based observations of the plasmaspheric plume and reconnection, *Science*, *343*, 1122–1125.
Weiss, L. A., R. L. Lambour, R. C. Elphic, and M. F. Thomsen (1997), Study of plasmaspheric evolution using geosynchronous observations and global modeling, *Geophys Res. Lett.*, *24*, 599–602, doi:10.1029/97GL00351.
Yahnin, A. G., and T. A. Yahnina (2007), Energetic proton precipitation related to ion-cyclotron waves, *J. Atmos. Sol. Terr. Phys.*, *69*, 1690–1706.
Yamamoto, T., K. Makita, and C.-I. Meng (1991), A particle simulation of large-amplitude undulations on the evening diffuse auroral boundary, *J. Geophys. Res.*, *96*, 1439–1449, doi:10.1029/90JA01984.
Yamamoto, T., M. Ozaki, S. Inoue, K. Makita, and C.-I. Meng (1994), Convective generation of "giant" undulations on the evening diffuse auroral boundary, *J. Geophys. Res.*, *99*, 19,499–19,512, doi:10.1029/94JA00273.
Yizengaw, E., J. Dewar, J. MacNeil, M. B. Moldwin, D. Galvin, J. Sanny, D. Berube, and B. Sandel (2008), The occurrence of ionospheric signatures of plasmaspheric plumes over different longitudinal sectors, *J. Geophys. Res.*, *113*, A08318, doi:10.1029/2007JA012925.